CMS Draft Analysis Note

The content of this note is intended for CMS internal use and distribution only

2017/09/04
Head Id: 422148
Archive Id: 423599
Archive Date: 2017/08/22
Archive Tag: trunk

Single top associated tW production at 13 TeV

A. Bharadwaj[2], S. Chenarani[4], J. Cuevas[1], J. R. González[1], D. Konstantinov[3], E. Palencia[1], P. Priyanka[2], K. Ranjan[2], I. Razumov[3], S. Sánchez Cruz[1], and P. Vischia (CCLE)[1]

[1] University of Oviedo, Spain
[2] University of Delhi, India
[3] IHEP, Russia
[4] School of Particles and Accelerators, IPM, Iran

Abstract

A study of the associated production of a single top quark and W boson in pp collisions at $\sqrt{s}$ = 13 TeV with the CMS experiment at the LHC is presented. The analyzed data corresponds to an integrated luminosity of 35.9 fb^{-1}. The measurement is performed using events with two leptons and a jet originated from a b quark. A multivariate analysis based on kinematic properties is utilized to separate the $t\bar{t}$ background from the signal. The observed signal has a significance of at least 6.6 σ and a cross section of 63.1 ± 1.8 (stat) ± 5.7 (syst) ± 2.1 (lum) pb, in agreement with the standard model expectation of 71.7 ± 1.8(scale) ± 3.4(PDF) pb.

Contents

1 Introduction

Electroweak production of single top quarks has been first observed by the CDF [1] and D0 [2] experiments at the Tevatron. Single-top-quark production proceeds mainly via three processes: the t-channel exchange of a virtual W boson, the s-channel production and decay of a virtual W boson, and the associated production of a top quark and a W boson (tW). The latter channel, which has a negligible production cross section at the Tevatron, represents a significant contribution to single-top-quark production at the Large Hadron Collider (LHC). Associated tW production is a very interesting production mechanism because of its interference with top quark pair production [3–5], its sensitivity to new physics [6–8] and its role as a background to SUSY and Higgs searches.

The tW channel was not accessible at the Tevatron due to its small cross-section in $p\overline{p}$ collisions at $\sqrt{s}$ = 1.96 TeV. At the LHC, however, evidence of this process with 7 TeV collision data was presented by the CMS [9] and ATLAS [10] Collaborations. With 8 TeV collision data, observations were made by the CMS [11] and the ATLAS [12] Collaborations with cross-section measurements in good agreement with theoretical predictions. The ATLAS Collaboration measured the production cross section using 13 TeV data [13]. This analysis note reports the first

study from the CMS experiment of tW production in pp collisions at $\sqrt{s}$ = 13 TeV. The measurement uses an integrated luminosity of $\mathcal{L}$ = 35.9 $\pm$ 0.9 fb^{-1}.

The production cross section for tW has been computed at approximate next-to-next-to-leading order, the theoretical prediction of the cross section for tW in pp collisions at $\sqrt{s}$ = 13 TeV, assuming a top-quark mass (m_t) of 172.5 GeV, is $71.7 \pm 1.8(\text{scale}) \pm 3.4(\text{PDF})$ pb [14], the first uncertainty corresponds to scale variation and the second to parton distribution function (pdf) sets. The leading order Feynman diagrams for tW production are shown in Fig. 1.

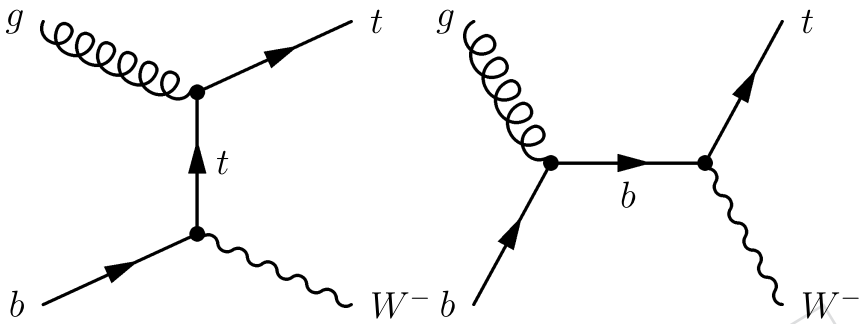

Figure 1: Leading order Feynman diagrams for single-top-quark production in the tW mode, the charge-conjugate modes are implicitly included.

The definition of tW production in perturbative QCD mixes with top quark pair production ($t\bar{t}$) at next-to-leading order (NLO) [3, 5, 15]. Two schemes are proposed to describe the tW signal: "diagram removal" (DR) [3], where all NLO diagrams which are doubly resonant, such as those in Fig. 2, are excluded from the signal definition; and "diagram subtraction" (DS) [3, 16], in which the differential cross section is modified with a gauge-invariant subtraction term, that locally cancels the contribution of $t\bar{t}$ diagrams. The DR scheme is used in this note, but it has been verified that the number of predicted events after full selection is consistent between the two approaches within the statistical uncertainties of the simulated samples. The differences are accounted for in the systematic uncertainties.

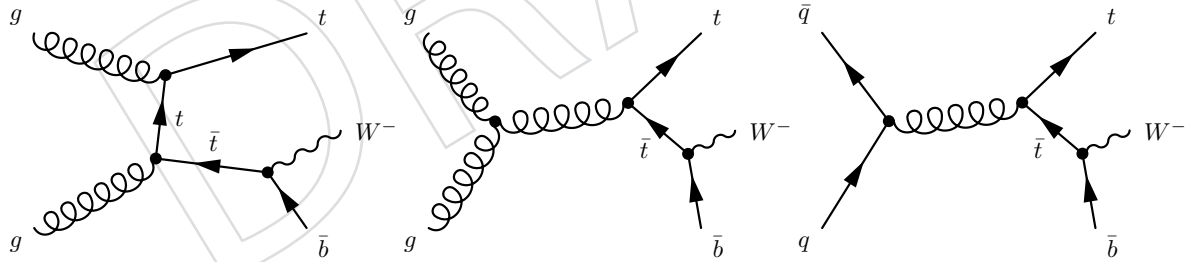

Figure 2: Feynman diagrams for tW single-top-quark production at next-to-leading order that are removed from the signal definition in the DR scheme, the charge-conjugate modes are implicitly included..

In the standard model, top quarks decay almost exclusively to a W boson and a b quark. The analysis is performed using the dilepton decay channels, in which the W boson produced in association with the top quark and the W boson from the decay of the top quark both decay leptonically into a muon or an electron, and a neutrino. This leads to a final state composed of two oppositely charged isolated leptons, a jet resulting from the fragmentation of a b quark, and two neutrinos. The neutrinos escape detection and are only discernible by the presence of missing transverse energy ($\not{E}_T$), defined as the magnitude of the vector sum of the transverse momentum of all reconstructed particles. The primary background to tW production in

this final state comes from $t\bar{t}$ production, with Z/γ^* events being the next most significant. The analysis uses a multivariate technique, exploiting kinematic and topological differences to distinguish the tW signal from the dominant $t\bar{t}$ background.

The analysis note is structured as follows. Section 2 gives a summary of the data and Monte Carlo samples used. The applied triggers, and the object and event selections are discussed in Sect. 3. Section 4 describes the determination of the Drell-Yan and the non-W/Z leptons backgrounds using data-driven methods. The description of the method used to separate the tW signal from the $t\bar{t}$ background is shown in Sect. 5. The different sources of systematic uncertainties are discussed in Sect. 6. and the tW production cross section extraction is described in Sect. 7. Conclusions and a summary of all results are given in Sect. 8.

2 Data and Monte Carlo samples

The data sets collected during the full LHC 2016 run at 13 TeV are listed in Tab. 1 and 2. From these data sets, certified runs are selected by applying the certified good-run lists as given in [17]. The total integrated luminosity corresponds to $\mathcal{L} = 35.9 \pm 0.9$ fb^{-1} [18].

The analysis has been carried out using the CMS event data model and the official software framework for event generation, simulation and reconstruction. (Data and Summer16 MC in CMSSW_8_0). Centrally provided MiniAODs generated with CMSSW_8_X_X are analyzed using release CMSSW_8_0_19. The data sets used are listed in Tabs. 3, 4 and 5.

The single top tW signal process is simulated using POWHEG v1 [19] with NNPDF 3.0 and PYTHIA 8.2 with the CUETP8M1 [20, 21] tune. The dilepton samples are used for the training of the BDTs (see Sect. 5) and the inclusive ones for the signal extraction. The WW, WZ, and ZZ diboson samples are produced using PYTHIA 8.2 with the CUETP8M1 tune.

The default POWHEG (v2) [22] setup with turning the damping parameter on (hdamp=172.5 GeV), is used to simulate $t\bar{t}$ events and its model dependencies on the top quark mass, the renormalization and factorization scale, Q^2, and the parton distribution functions (PDFs). NNPDF 3.0 is used as default PDF. In case of the nominal sample, the $t\bar{t}$ events were showered using PYTHIA 8.2 [23, 24] with the CUETP8M2T4 tune [25]. To study the effect from a different model of hadronization and parton fragmentation, the default POWHEG sample is also interfaced to HERWIG++ [26] with the EE5C tune. An alternative $t\bar{t}$ sample is generated using MG5_AMC@NLO 2.2.2 [27] including MADSPIN [28] with NNPDF 3.0 [29] and PYTHIA 8.2 with the CUETP8M2T4 tune for parton showering. These $t\bar{t}$ events are generated with up to two additional partons at next-to-leading-order, and the FxFx scheme [30] is used for the merging of the different jet multiplicities.

Besides the $t\bar{t}$ background process, other background contributions (Drell/Yan background (Z+jets) and diboson events (WW, WZ, and ZZ) with multiple jets) are taken from MC simulations. Additional background contamination comes from events in which a jet is misidentified as an electron or the production of heavy hadrons that decay into leptons which pass the isolation requirements. This last type of background is dominated by non-dileptonic $t\bar{t}$ events as well as W+jets and further discussed in Section 4.

The Z+jets background samples are generated with MG5_AMC@NLO 2.2.2 with NNPDF 3.0 and interfaced to PYTHIA 8.2 with the CUETP8M1 tune for hadronization and fragmentation. Z-bosons are simulated with up to two additional partons and the FxFx scheme is used for merging. The generation is split into two distinct Z/γ^* invariant mass ranges: 10-50 GeV and > 50 GeV.

Table 1: Collision data samples used in the analysis (I).

Data set	Events	Luminosity
/SingleMuon/Run2016B-03Feb2017_ver2-v2/MINIAOD	158,145,722	
/SingleElectron/Run2016B-03Feb2017_ver2-v2/MINIAOD	246,440,440	
/MuonEG/Run2016B-03Feb2017_ver2-v2/MINIAOD	32,727,796	5.78
/DoubleMuon/Run2016B-03Feb2017_ver2-v2/MINIAOD	82,535,526	
/DoubleEG/Run2016B-03Feb2017_ver2-v2/MINIAOD	143,073,268	
/SingleMuon/Run2016C-03Feb2017-v1/MINIAOD	67,441,308	
/SingleElectron/Run2016C-03Feb2017-v1/MINIAOD	97,259,854	
/MuonEG/Run2016C-03Feb2017-v1/MINIAOD	15,405,678	2.56
/DoubleMuon/Run2016C-03Feb2017-v1/MINIAOD	27,934,629	
/DoubleEG/Run2016C-03Feb2017-v1/MINIAOD	47,677,856	
/SingleMuon/Run2016D-03Feb2017-v1/MINIAOD	98,017,996	
/SingleElectron/Run2016D-03Feb2017-v1/MINIAOD	148,167,727	
/MuonEG/Run2016D-03Feb2017-v1/MINIAOD	23,482,352	4.25
/DoubleMuon/Run2016D-03Feb2017-v1/MINIAOD	33,861,745	
/DoubleEG/Run2016D-03Feb2017-v1/MINIAOD	53,324,960	
/SingleMuon/Run2016E-03Feb2017-v1/MINIAOD	90,963,495	
/SingleElectron/Run2016E-03Feb2017-v1/MINIAOD	117,321,545	
/MuonEG/Run2016E-03Feb2017-v1/MINIAOD	22,519,303	4.01
/DoubleMuon/Run2016E-03Feb2017-v1/MINIAOD	28,246,946	
/DoubleEG/Run2016E-03Feb2017-v1/MINIAOD	49,877,710	
/SingleMuon/Run2016F-03Feb2017-v1/MINIAOD	65,489,554	
/SingleElectron/Run2016F-03Feb2017-v1/MINIAOD	70,593,532	
/MuonEG/Run2016F-03Feb2017-v1/MINIAOD	16,002,165	3.10
/DoubleMuon/Run2016F-03Feb2017-v1/MINIAOD	20,329,921	
/DoubleEG/Run2016F-03Feb2017-v1/MINIAOD	34,577,629	
/SingleMuon/Run2016G-03Feb2017-v1/MINIAOD	149,916,849	
/SingleElectron/Run2016G-03Feb2017-v1/MINIAOD	153,330,123	
/MuonEG/Run2016G-03Feb2017-v1/MINIAOD	33,854,612	7.54
/DoubleMuon/Run2016G-03Feb2017-v1/MINIAOD	45,235,604	
/DoubleEG/Run2016G-03Feb2017-v1/MINIAOD	78,764,716	
/SingleMuon/Run2016H-03Feb2017_ver2-v1/MINIAOD	169,642,135	
/SingleElectron/Run2016H-03Feb2017_ver2-v1/MINIAOD	125,826,667	
/MuonEG/Run2016H-03Feb2017_ver2-v1/MINIAOD	28,466,022	8.39
/DoubleMuon/Run2016H-03Feb2017_ver2-v1/MINIAOD	47,693,168	
/DoubleEG/Run2016H-03Feb2017_ver2-v1/MINIAOD	83,361,083	

Table 3 shows, for completeness, the FxFx and MLM samples for DY and W+jets. In the analysis, FxFx is used for DY and MLM for W+jets.

For comparison with the measured distributions, the event yields in the simulated samples are normalised to the corresponding integrated luminosity and their theoretical cross sections. These are taken from next-to-next-to-leading-order (NNLO) (W+jets and Z/γ^*+jets), NLO plus next-to-next-to-leading-log (NNLL) (single-top-quark tW-channels [31]), NLO (diboson [32]) calculations. For the simulated $t\bar{t}$ sample, the full NNLO+NNLL calculation, performed with the TOP++ 2.0 program [33], is used. The PDF and α_S uncertainties are estimated using the PDF4LHC prescription [34, 35] with the MSTW2008nnlo68cl [36], CT10 NNLO [37, 38], and NNPDF2.3 5f FFN [29] PDF sets, and added in quadrature to the scale uncertainty to obtain

Table 2: Collision data samples used in the analysis (II).

Data set	Events	Luminosity
/SingleMuon/Run2016H-03Feb2017_ver3-v1/MINIAOD	4,393,029	
/SingleElectron/Run2016H-03Feb2017_ver3-v1/MINIAOD	3,191,585	
/MuonEG/Run2016H-03Feb2017_ver3-v1/MINIAOD	770,494	0.22
/DoubleMuon/Run2016H-03Feb2017_ver3-v1/MINIAOD	1,219,644	
/DoubleEG/Run2016H-03Feb2017_ver3-v1/MINIAOD	2,027,651	

a $t\bar{t}$ production cross section of $832\ ^{+20}_{-29}\,(\text{scale}) \pm 35(\text{PDF} + \alpha_s)$ pb assuming a top-quark mass value of 172.5 GeV.

3 Description of the event selection

3.1 Trigger selection

In the CMS design, the real time selection of events is achieved in two physical steps, namely the fast Level-1 Trigger and the High-Level Trigger (HLT) operating on longer timescales. The Level-1 trigger is built of mostly hardware level information of the detectors while the HLT selection is implemented as a sequence of reconstruction and filter steps of increasing complexity. High Level inclusive triggers designed to select events in the dilepton channel have been considered, namely

For MC and data (Runs B to G):

- $e^{\pm}\mu^{\mp}$: `HLT_Ele27_WPTight_Gsf_v* || HLT_IsoMu24_v* || HLT_IsoTkMu24_v* || HLT_Mu8_TrkIsoVVL_Ele23_CaloIdL_TrackIdL_IsoVL_v* || HLT_Mu23_TrkIsoVVL_Ele12_CaloIdL_TrackIdL_IsoVL_v*`
- $e^{+}e^{-}$: `HLT_Ele23_Ele12_CaloIdL_TrackIdL_IsoVL_DZ_v* || HLT_Ele27_WPTight_Gsf_v*`
- $\mu^{+}\mu^{-}$: `HLT_Mu17_TrkIsoVVL_Mu8_TrkIsoVVl_v* || HLT_Mu17_TrkIsoVVL_TkMu8_TrkIsoVVL_v* || HLT_IsoMu24_v* || HLT_IsoTkMu24_v*`

For data (Run H):

- $e^{\pm}\mu^{\mp}$: `HLT_Ele27_WPTight_Gsf_v* || HLT_IsoMu24_v* || HLT_IsoTkMu24_v* || HLT_Mu8_TrkIsoVVL_Ele23_CaloIdL_TrackIdL_IsoVL_DZ_v* || HLT_Mu23_TrkIsoVVL_Ele12_CaloIdL_TrackIdL_IsoVL_DZ_v*`
- $e^{+}e^{-}$: same as above, `HLT_Ele23_Ele12_CaloIdL_TrackIdL_IsoVL_DZ_v* || HLT_Ele27_WPTight_Gsf_v*`
- $\mu^{+}\mu^{-}$: `HLT_Mu17_TrkIsoVVL_Mu8_TrkIsoVVl_DZ_v* || HLT_Mu17_TrkIsoVVL_TkMu8_TrkIsoVVL_DZ_v* || HLT_IsoMu24_v* || HLT_IsoTkMu24_v*`

3.2 Reconstruction of signal and background events

The tW dilepton final state is characterized by the presence of a high-p_{T} isolated lepton (electron, muon) pair associated with missing transverse energy $\not\!\!E_T$ and 1 b-quark jet. The reconstruction of the different objects is based on the Particle-Flow (PF) algorithm [39].

3.2.1 Selection of electrons

The selection criteria for electron candidates are:

- $p_{\mathrm{T}} > 20$ GeV and $|\eta| < 2.4$;

Table 3: Simulated data samples used in this analysis, together with the cross section assigned to each process and number of events processed.
(*/RunIISummer16MiniAODv2-PUMoriond17_80X_mcRun2_asymptotic_2016_TrancheIV_v6-v1)

Sample	σ [pb]	Events
/TT_TuneCUETP8M2T4_13TeV-powheg-pythia8	831.8	77,229,341
/TT_TuneCUETP8M2T4_13TeV-powheg-pythia8 (_backup)	831.8	78,006,311
/TTTo2L2Nu_TuneCUETP8M2_ttHtranche3_13TeV-powheg-pythia8	831.8	79,092,400
/ST_tW_top_5f_inclusiveDecays_13TeV-powheg-pythia8_TuneCUETP8M1 (_ext1-v1)	35.85	6,952,830
/ST_tW_antitop_5f_inclusiveDecays_13TeV-powheg-pythia8_TuneCUETP8M1 (_ext1-v1)	35.85	6,933,094
/ST_tW_top_5f_NoFullyHadronicDecays_13TeV-powheg_TuneCUETP8M1	19.467	5,372,991
/ST_tW_top_5f_NoFullyHadronicDecays_13TeV-powheg_TuneCUETP8M1 (_ext1-v1)	19.467	3,256,650
/ST_tW_top_5f_NoFullyHadronicDecays_13TeV-powheg_TuneCUETP8M1 (_ext2-v2)	19.467	2,715,978
/ST_tW_antitop_5f_NoFullyHadronicDecays_13TeV-powheg_TuneCUETP8M1	19.467	5,425,134
/ST_tW_antitop_5f_NoFullyHadronicDecays_13TeV-powheg_TuneCUETP8M1 (_ext1-v1)	19.467	3,256,407
/ST_tW_antitop_5f_NoFullyHadronicDecays_13TeV-powheg_TuneCUETP8M1 (_ext2-v1)	19.467	2,726,603
/WW_TuneCUETP8M1_13TeV-pythia8 (_ext1-v1)	115.0	6,987,124
/ZZ_TuneCUETP8M1_13TeV-pythia8 (_ext1-v1)	16.5	998,034
/WZ_TuneCUETP8M1_13TeV-pythia8 (_ext1-v1)	47.1	2,995,828
/WJetsToLNu_TuneCUETP8M1_13TeV-amcatnloFXFX-pythia8	61526.7	24,028,465
/WJetsToLNu_TuneCUETP8M1_13TeV-madgraphMLM-pythia8	61526.7	29,705,748
/WJetsToLNu_TuneCUETP8M1_13TeV-madgraphMLM-pythia8 (_ext2-v1)	61526.7	57,026,058
/DYJetsToLL_M-10to50_TuneCUETP8M1_13TeV-amcatnloFXFX-pythia8	22635.1	30,920,596
/DYJetsToLL_M-10to50_TuneCUETP8M1_13TeV-amcatnloFXFX-pythia8 (_ext1-v1)	22635.1	40,381,391
/DYJetsToLL_M-50_TuneCUETP8M1_13TeV-amcatnloFXFX-pythia8 (_ext2-v1)	6025.2	122,055,388
/DYJetsToLL_M-10to50_TuneCUETP8M1_13TeV-madgraphMLM-pythia8	22635.1	35,291,566
/DYJetsToLL_M-50_TuneCUETP8M1_13TeV-madgraphMLM-pythia8 (_ext1-v2)	6025.2	49,144,274
/DYJetsToLL_M-50_TuneCUETP8M1_13TeV-madgraphMLM-pythia8 (_ext2-v1)	6025.2	96,658,943
/TTWJetsToLNu_TuneCUETP8M1_13TeV-amcatnloFXFX-madspin-pythia8 (_ext1-v3)	0.2043	2,160,168
/TTWJetsToLNu_TuneCUETP8M1_13TeV-amcatnloFXFX-madspin-pythia8 (_ext2-v1)	0.2043	3,120,397
/TTWJetsToQQ_TuneCUETP8M1_13TeV-amcatnloFXFX-madspin-pythia8	0.40620	833,298
/TTZToQQ_TuneCUETP8M1_13TeV-amcatnlo-pythia8	0.5297	749,400
/TTZToLLNuNu_M-10_TuneCUETP8M1_13TeV-amcatnlo-pythia8 (_ext1-v1)	0.253	1,992,438
/TTZToLLNuNu_M-10_TuneCUETP8M1_13TeV-amcatnlo-pythia8 (_ext2-v1)	0.253	5,982,035

- veto of the transition region $1.4442 < |\eta_{SuCluster}| < 1.5660$;
- cut based tight ID (SPRING16_25ns_v1), as detailed in Ref. [40], for a high purity sample.
- relative electron isolation (REI): the isolation is computed following the equation below, considering iso deposits in a cone of $\Delta R < 0.3$. Pile up is taken into account by using an effective area correction.

$$REI = \frac{(ChargedHadronIso + NeutralHadronIso + PhotonIso)}{p_T(e)}$$

3.2.2 Selection of muons

The selection criteria for muon candidates are (tight muon ID [41]):

- $p_T > 20$ GeV and $|\eta| < 2.4$;
- is a GlobalMuon and PFMuon;
- number of matchedStations > 1;

Table 4: Simulated signal samples used in this analysis for the estimation of some systematic uncertainties, together with the number of events processed.
(*/RunIISummer16MiniAODv2-PUMoriond17_80X_mcRun2_asymptotic_2016_TrancheIV_v6-v1)

Sample	Events
/ST_tW_top_5f_DS_NoFullyHadronicDecays_13TeV-powheg-pythia8_TuneCUETP8M1	3,192,627
/ST_tW_antitop_5f_DS_NoFullyHadronicDecays_13TeV-powheg-pythia8	3,257,313
/ST_tW_top_5f_mtop1695_NoFullyHadronicDecays_13TeV-powheg-pythia8	3,199,011
/ST_tW_top_5f_mtop1755_NoFullyHadronicDecays_13TeV-powheg-pythia8	2,958,559
/ST_tW_antitop_5f_mtop1695_NoFullyHadronicDecays_13TeV-powheg-pythia8	3,028,578
/ST_tW_antitop_5f_mtop1755_NoFullyHadronicDecays_13TeV-powheg-pythia8	3,253,487
/ST_tW_top_5f_PSscaleup_NoFullyHadronicDecays_13TeV-powheg-pythia8	3,124,934
/ST_tW_top_PSscaledown_5f_NoFullyHadronicDecays_13TeV-powheg-pythia8	3,181,663
/ST_tW_antitop_5f_PSscaleup_NoFullyHadronicDecays_13TeV-powheg-pythia8	1,628,527
/ST_tW_antitop_PSscaledown_5f_NoFullyHadronicDecays_13TeV-powheg-pythia8	1,628,344
/ST_tW_top_5f_isrup_NoFullyHadronicDecays_13TeV-powheg	3,129,831
/ST_tW_top_isrdown_5f_NoFullyHadronicDecays_13TeV-powheg	3,201,658
/ST_tW_top_5f_fsrup_NoFullyHadronicDecays_13TeV-powheg	3,212,416
/ST_tW_top_fsrdown_5f_NoFullyHadronicDecays_13TeV-powheg	2,975,405
/ST_tW_antitop_5f_isrup_NoFullyHadronicDecays_13TeV-powheg	3,076,356
/ST_tW_antitop_isrdown_5f_NoFullyHadronicDecays_13TeV-powheg	3,101,414
/ST_tW_antitop_5f_fsrup_NoFullyHadronicDecays_13TeV-powheg	3,001,597
/ST_tW_antitop_fsrdown_5f_NoFullyHadronicDecays_13TeV-powheg	3,235,062
/ST_tW_top_5f_MEscaleup_NoFullyHadronicDecays_13TeV-powheg	3,188,774
/ST_tW_top_MEscaledown_5f_NoFullyHadronicDecays_13TeV-powheg	3,052,085
/ST_tW_antitop_5f_MEscaleup_NoFullyHadronicDecays_13TeV-powheg	1,607,001
/ST_tW_antitop_MEscaledown_5f_NoFullyHadronicDecays_13TeV-powheg	1,575,183
/ST_tW_top_5f_NoFullyHadronicDecays_13TeV-powheg_herwigpp	3,201,087
/ST_tW_antitop_5f_NoFullyHadronicDecays_13TeV-powheg_herwigpp	3,216,427

- number of valid pixel hits > 0;
- number of valid hits in the inner tracker > 5;
- number of muon hits > 0;
- $\chi^2/ndof < 10$ for the global muon fit;
- transverse impact parameter w.r.t. the beam spot < 0.2 cm and dZ< 0.5 cm, applied on the track from the inner tracker;
- relative muon isolation (RMI) < 0.15, based on particle flow candidates, defined as

$$RMI = \frac{(ChargedHadronIso + NeutralHadronIso + PhotonIso)}{p_T(\mu)}$$

Each component is computed using PF isodeposits in a cone of 0.4 around the muon direction, where charged PF candidates from PU events are removed (PF charged subtraction). $p_T(\mu)$ represents the transverse momentum of the muon. Delta-β corrections are applied.

3.2.3 Selection of jets

The jets are reconstructed using PF candidates (without considering the charged PF particles coming from PU) with the anti-kT algorithm within an opening angle of 0.4. The selection

Table 5: Simulated $t\bar{t}$ background samples used in this analysis for the estimation of some systematic uncertainties, together with the number of events processed.
(`*/RunIISummer16MiniAODv2-PUMoriond17_80X_mcRun2_asymptotic_2016_TrancheIV_v6-v1`)

Sample	Events
`/TT_TuneCUETP8M2T4_13TeV-powheg-isrdown-pythia8`	29,084,029
`/TT_TuneCUETP8M2T4_13TeV-powheg-isrdown-pythia8 (_ext1-v1)`	29,915,551
`/TT_TuneCUETP8M2T4_13TeV-powheg-isrup-pythia8 (_ext1-v1)`	59,033,604
`/TT_TuneCUETP8M2T4_13TeV-powheg-fsrdown-pythia8`	29,716,580
`/TT_TuneCUETP8M2T4_13TeV-powheg-fsrdown-pythia8 (_ext1-v1)`	29,590,326
`/TT_TuneCUETP8M2T4_13TeV-powheg-fsrup-pythia8`	29,777,488
`/TT_TuneCUETP8M2T4_13TeV-powheg-fsrup-pythia8 (_ext1-v1)`	29,453,411
`/TT_hdampDOWN_TuneCUETP8M2T4_13TeV-powheg-pythia8`	29,117,820
`/TT_hdampDOWN_TuneCUETP8M2T4_13TeV-powheg-pythia8 (_ext1-v1)`	29,046,156
`/TT_hdampUP_TuneCUETP8M2T4_13TeV-powheg-pythia8`	29,689,380
`/TT_hdampUP_TuneCUETP8M2T4_13TeV-powheg-pythia8 (_ext1-v1)`	29,169,226
`/TT_TuneCUETP8M2T4up_13TeV-powheg-pythia8`	29,310,620
`/TT_TuneCUETP8M2T4down_13TeV-powheg-pythia8`	28,354,188
`/TT_TuneCUETP8M2T4_mtop1665_13TeV-powheg-pythia8`	19,380,254
`/TT_TuneCUETP8M2T4_mtop1695_13TeV-powheg-pythia8 (_backup)`	29,173,030
`/TT_TuneCUETP8M2T4_mtop1695_13TeV-powheg-pythia8 (_ext1-v1)`	9,954,200
`/TT_TuneCUETP8M2T4_mtop1695_13TeV-powheg-pythia8 (_ext2-v1)`	19,415,360
`/TT_TuneCUETP8M2T4_mtop1715_13TeV-powheg-pythia8`	19,578,812
`/TT_TuneCUETP8M2T4_mtop1735_13TeV-powheg-pythia8`	19,419,050
`/TT_TuneCUETP8M2T4_mtop1755_13TeV-powheg-pythia8`	29,459,232
`/TT_TuneCUETP8M2T4_mtop1755_13TeV-powheg-pythia8 (_ext1-v1)`	9,930,052
`/TT_TuneCUETP8M2T4_mtop1755_13TeV-powheg-pythia8 (_ext2-v1)`	19,995,376
`/TT_TuneCUETP8M2T4_mtop1785_13TeV-powheg-pythia8`	16,377,176
`/TT_TuneCUETP8M2T4_erdON_13TeV-powheg-pythia8`	29,943,330
`/TT_TuneCUETP8M2T4_erdON_13TeV-powheg-pythia8 (_ext1-v1)`	29,938,880
`/TT_TuneCUETP8M2T4_QCDbasedCRTune_erdON_13TeV-powheg-pythia8`	29,983,790
`/TT_TuneCUETP8M2T4_QCDbasedCRTune_erdON_13TeV-powheg-pythia8 (_ext1-v1)`	29,636,416
`/TT_TuneCUETP8M2T4_GluonMoveCRTune_13TeV-powheg-pythia8`	59,037,234
`/TT_TuneCUETP8M2T4_GluonMoveCRTune_erdON_13TeV-powheg-pythia8`	56,168,970
`/TTJets_TuneCUETP8M2T4_13TeV-amcatnloFXFX-pythia8`	43,561,608
`/TT_TuneEE5C_13TeV-powheg-herwigpp`	29,412,687
`/TT_TuneEE5C_13TeV-powheg-herwigpp (_ext2-v1)`	19,762,915

criteria for jet candidates are:

- L1Fastjet corrections compatible with PFnoPU, Level 2 and Level 3 jet energy corrections and L2L3Residual corrections for data. The latest set of JECs (Summer16_23Sep2016V3_MC and Summer16_23Sep2016V3_DATA) are used;
- $p_{\mathrm{T}} > 30$ GeV and $|\eta| < 2.4$;
- loose jet identification [42], which corresponds to a fraction of neutral hadronic energy <0.99, a fraction of neutral electromagnetic energy <0.99, and number of constituents >1 for jets with $|\eta| < 2.7$. On top of that, if $|\eta| < 2.4$, we require a fraction of charged hadronic energy >0, charge multiplicity >0 and a fraction of charged electromagnetic energy <0.99;

- instead of using PF top projection for lepton removal, we apply a jet lepton cleaning: exclusion of jets overlapping with fully selected leptons (electron/muon) used in the analysis if $\Delta R(jet, lepton) < 0.4$).

3.2.4 Identification of b-quark jets

As tW signal events have one jet originating from a b quark, the Combined Secondary Vertex tagger (CSVv2) is used to improve the background rejection. The medium working point (CSVv2M = 0.8484) is used in order to optimize the efficiency and background rejection without introducing larger uncertainties.

3.2.5 Missing transverse energy

This analysis uses corrected ("Type-1") $\not\!\!E_T$. Several filters rejecting events where known $\not\!\!E_T$ problems were present have been applied. In order to reduce the instrumental noise in the detector, the following filters are applied: primary vertex, CSC beam halo, HBHE noise, HBHEiso noise, eebadSC, and Ecal TP. The detailed description of these filters can be found in the official page of the MET POG [43].

3.3 Event selection

The selection is based in the requirements given in Ref. [44]. $t\bar{t}$ events are classified as belonging to the $e^{\pm}\mu^{\mp}$, $\mu^+\mu^-$ or e^+e^- final state if the two leading leptons of good quality are an electron and a muon, two muons or two electrons, respectively. This includes also electrons and muons from a τ lepton decay. We require the leading lepton to have $p_T > 25$ GeV. In a second step, events are rejected if these two leptons are not of opposite charge. To reduce the contamination from Drell-Yan background, the invariant mass of the lepton pair is required to be greater than 20 GeV. On top of that, exactly one good jet is required to be present in the event and this jet has to be identified as a b-jet. Events with 2 jets and 1 b-tag and/or 2 jets and 2 b-tags are also considered.

For the same flavour channels (e^+e^-, $\mu^+\mu^-$) we also require:

- the missing transverse energy in the event to be larger than 40 GeV
- the invariant mass of the lepton pair to be 15 GeV away of the Z pole mass

in order to further suppress the DY contamination.

The $\mu^+\mu^-$ and e^+e^- channels are included in this document for completeness but will not be used in the analysis.

3.4 Event reweighting

3.4.1 Pileup

The target pileup distribution for data is generated using the instantaneous luminosity per bunch crossing for each luminosity section, stored in the LumiDB database, and the total pp inelastic cross section.A Poisson smearing is applied to model statistical fluctuations. The source distribution is taken from the PileupInfo collection which stores the true number of pileup events mixed with the particular hard interaction process in each MC event. A variation of $\pm 4.6\%$ on the minimum bias cross section is used to estimate the uncertainties due to pileup modeling [45].

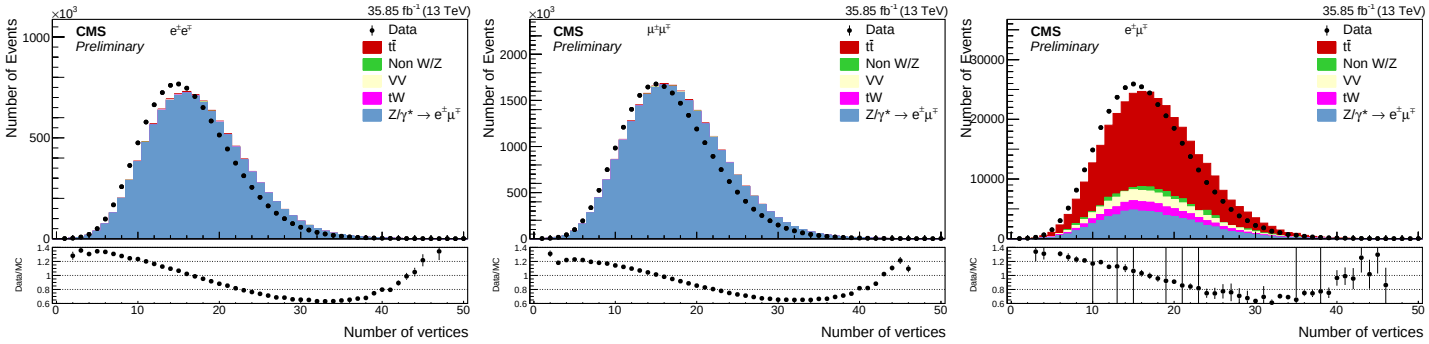

Figure 3: Distribution of the number of good vertices in the event.

3.4.2 Trigger

Scales factors derived in [46] are used, see Fig. 4.

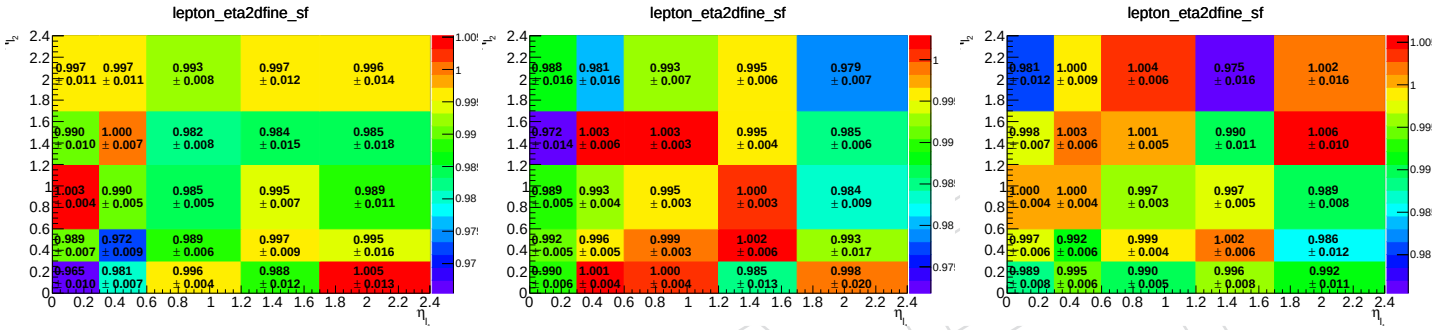

Figure 4: Trigger SFs.

3.4.3 Lepton Id/Iso

Official muon [47] and electron [48] SFs from POG are used (see Figs. 5 and 6). In particular:

- Muon tracking efficiency:
  `https://test-calderona.web.cern.ch/test-calderona/MuonPOG/2016dataReRecoEfficiencies/tracking/Tracking_EfficienciesAndSF_BCDEFGH.root`
- Muon tight Id (B - F):
  `https://gaperrin.web.cern.ch/gaperrin/tnp/TnP2016/2016Data_Moriond2017_6_12_16/JSON/RunBCDEF/EfficienciesAndSF_BCDEF.root`
  (histogram MC_NUM_tightID_DEN_genTracks_PAR_pt_eta/abseta_pt_ratio)
- Muon tight Id (G - H):
  `https://gaperrin.web.cern.ch/gaperrin/tnp/TnP2016/2016Data_Moriond2017_6_12_16/JSON/RunGH/EfficienciesAndSF_GH.root`
  (histogram MC_NUM_tightID_DEN_genTracks_PAR_pt_eta/abseta_pt_ratio)
- Muon tight isolation (B - F):
  `https://test-calderona.web.cern.ch/test-calderona/MuonPOG/2016dataReRecoEfficiencies/isolation/EfficienciesAndSF_BCDEF.root` (histogram tightISO_TightID_pt_eta/abseta_pt_ratio)
- Muon tight isolation (G - H):
  `https://test-calderona.web.cern.ch/test-calderona/MuonPOG/2016dataReRecoEfficiencies/isolation/EfficienciesAndSF_GH.root` (histogram tightISO_TightID_pt_eta/abseta_pt_ratio)
- Electron reconstruction efficiency:
  `http://fcouderc.web.cern.ch/fcouderc/EGamma/scaleFactors/Moriond17/approval/RECO/passingRECO/egammaEffi.txt_EGM2D.root` (histogram EGamma_SF2D)

- Electron Id/Isolation:
  `http://fcouderc.web.cern.ch/fcouderc/EGamma/scaleFactors/Moriond17/approval/EleID/passingTight80X/egammaEffi.txt_EGM2D.root` (histogram EGamma_SF2D)

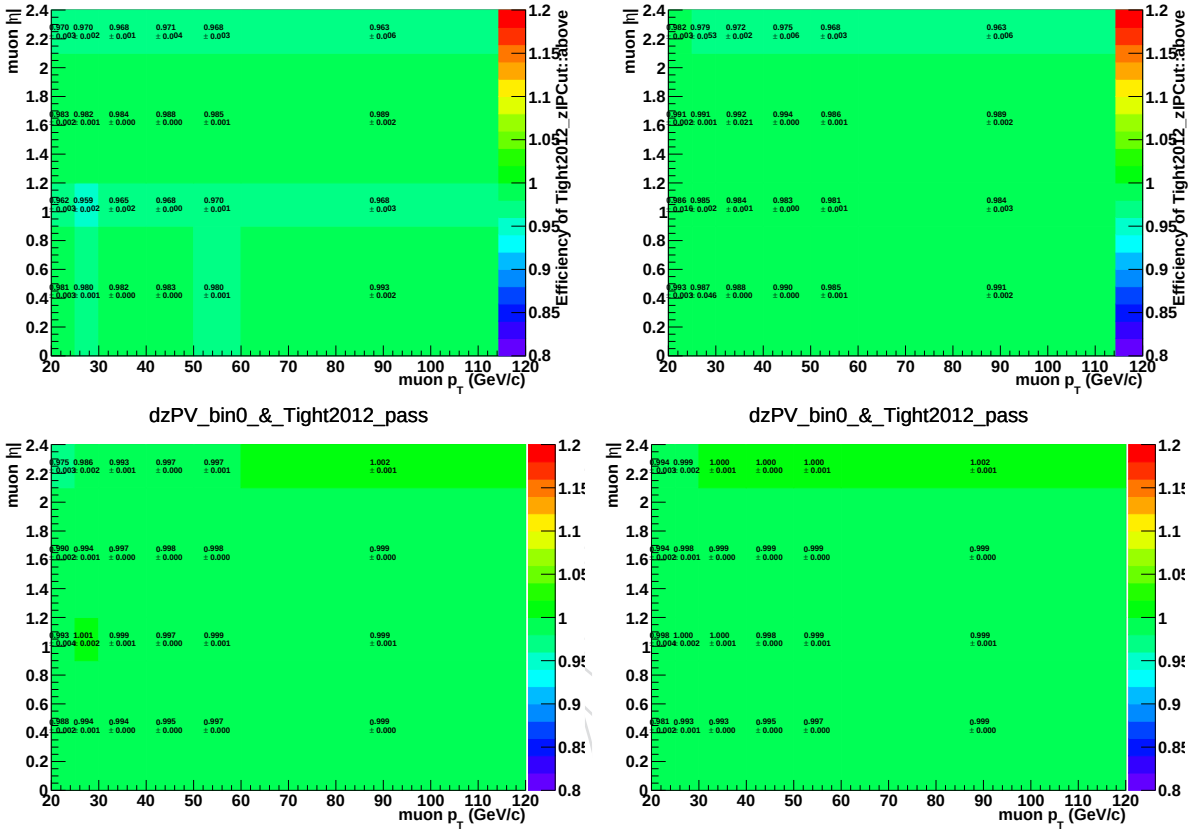

Figure 5: Muon identification (top) and isolation (bottom) SFs for run eras B-F (left) and G-H (right).

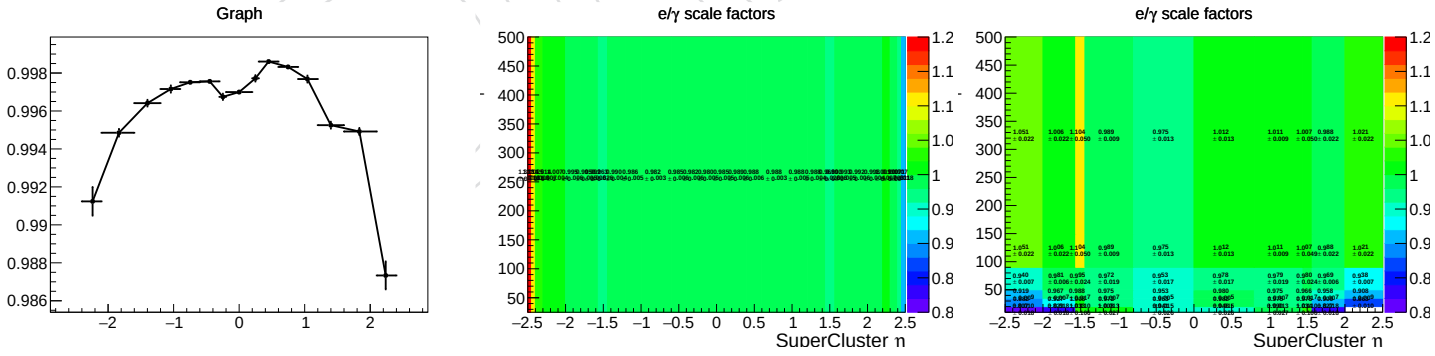

Figure 6: Muon tracker efficiency (left), electron reconstruction efficiency (center), and electron identification and isolation (right) SFs.

3.4.4 B-tagging

As the MC does not reproduce completely the *b*-tagging performance in data, the officially recomended data-to-MC scale factors [49] are applied:

- https://twiki.cern.ch/twiki/pub/CMS/BtagRecommendation80XReReco/CSVv2_Moriond17_B_H.csv

3.5 Yields

The expected yields after applying the object and event selection described above are shown in Tab. 6. Figures 7 and 8 show a data-MC for several kinematic variables at dilepton level. In general, very good agreement is observed.

Table 6: Total number of events observed in data and the number of signal and background events expected from simulation at 13 TeV.

Source	Dilepton	1j1b	2j1b	2j2b
Drell-Yan	67803	558	294	14
Non W/Z leptons	6190	153	361	52
Dibosons	27350	210	118	10
$t\bar{t}$ V	619	20	60	18
$t\bar{t}$ dilepton	234979	30615	48237	25143
Single top quark	23455	6171	3134	731
Total	360399	37727	52201	25968
Data	357237	36606	50960	25704

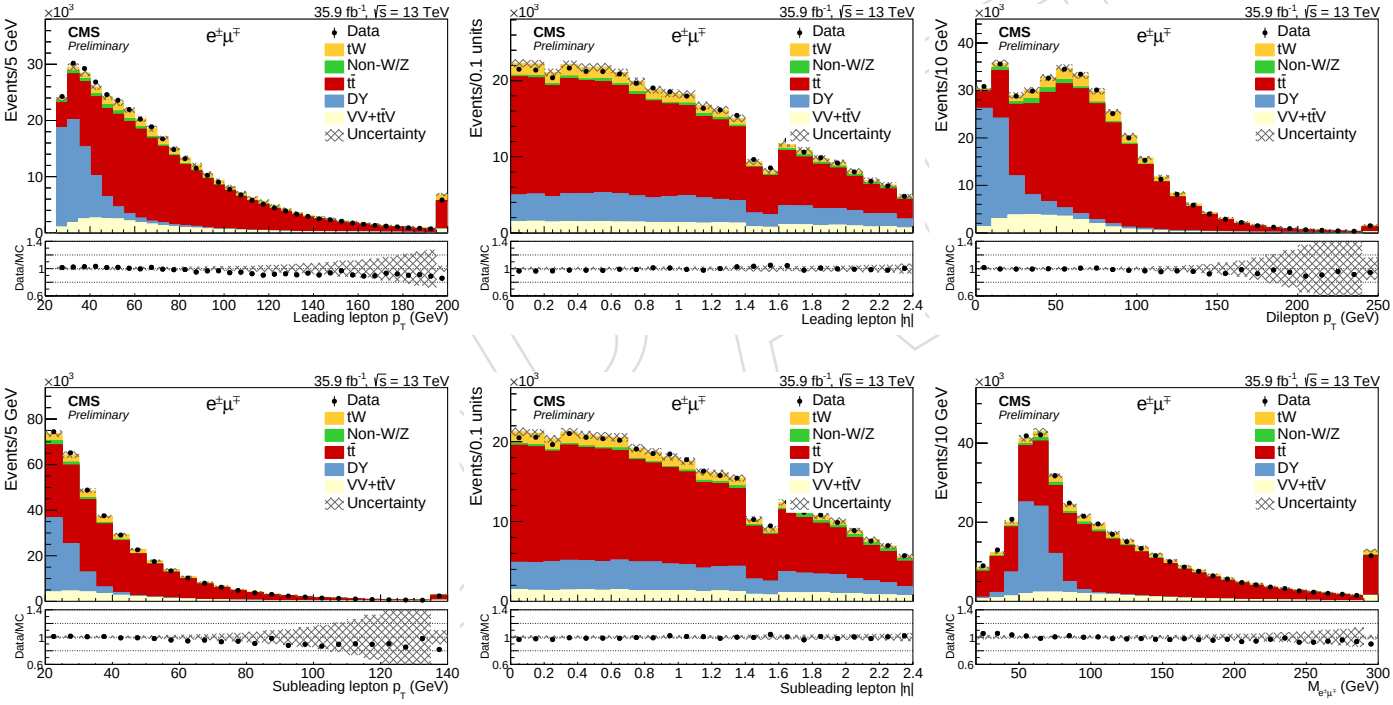

Figure 7: Data-MC comparison for several lepton kinematic variables at dilepton level.

As expected, the amount of signal is tiny in comparison with the overhelming $t\bar{t}$ background and a cut based analysis is extremely challenging. Therefore, a multivariate analysis will be pursued, see Sect. 5.

In order to gain discrimination power, signal regions where the presence of signal events is larger are used. In particular, as shown in Fig. 9, events with exactly one jet which is b-tagged (1j1b), and with exactly 2 jets with one of them b-tagged (2j1b) show a reasonable signal to background ratio and will be used separately to perform the signal extraction.

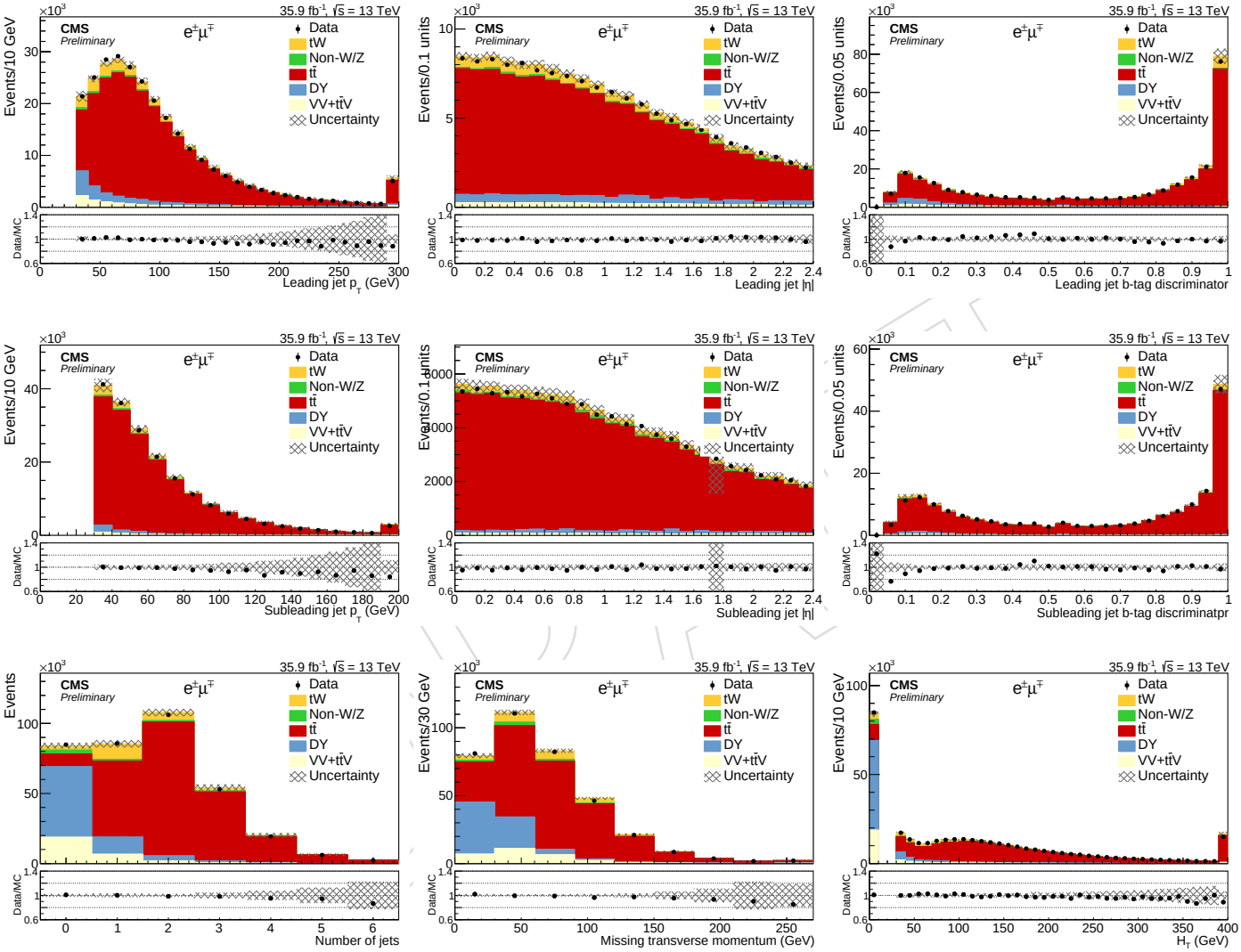

Figure 8: Data-MC comparison for several jet kinematic variables at dilepton level.

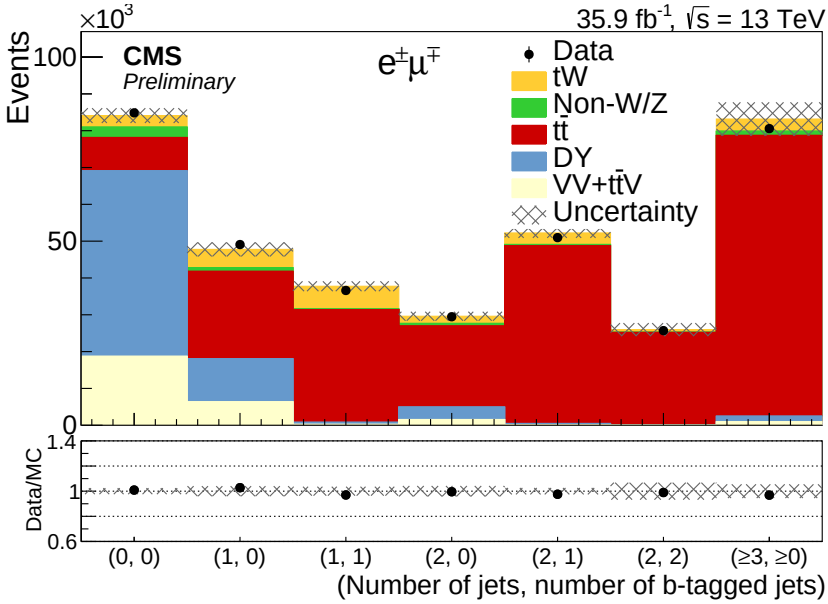

Figure 9: njetsnbtags distribution

4 Background estimation

In this section we describe the evaluation of the backgrounds that may contaminate our signal.

4.1 Drell-Yan background

The events containing a Z boson can be an important background in the dilepton final states. To evaluate this background we use a data-driven procedure [9]. The events rejected by the Z veto ($76 < M_{\ell\ell} < 106$ GeV) are used to estimate the Drell-Yan contribution in the dilepton channels. The number of events passing the Z veto is equal to the ratio of outside Z-peak window to inside Z-peak window events derived from simulation in an estimation of the Drell-Yan contribution near the dilepton mass peak:

$$N^{estimated}_{\ell\ell,out} = \frac{N^{DYMC}_{\ell\ell,out}}{N^{DYMC}_{\ell\ell,in}}.(N^{observed}_{\ell\ell,in} - \frac{1}{2}k_{\ell\ell}.N^{observed}_{e\mu,in}),$$

where $N^{observed}_{ee,in}$ and $N^{observed}_{\mu\mu,in}$ are estimated from the number of all events failling the Z veto requirement, after subtraction of non Drell-Yan contribution estimated from $e^{\pm}\mu^{\mp}$ events passing the same selection. The k factor $k_{\ell\ell}$ corrects difference in acceptance and reconstruction efficiencies between electrons and muons and is calculated using the events in the Z-peak window passing the standard dilepton and jet selection but without any $\not{E}_T$cut, and can be expressed as:

$$k_{ee} = \sqrt{\frac{N^{loose}_{ee,in}}{N^{loose}_{\mu\mu,in}}}, k_{\mu\mu} = \sqrt{\frac{N^{loose}_{\mu\mu,in}}{N^{loose}_{ee,in}}}$$

Using the full 13TeV data samples we get Drell-Yan estimation at the 1j1b level for the e^+e^- and $\mu^+\mu^-$ channels, the data-driven estimation is then compared to the MC simulation for derive a scale factor (SF) for e^+e^- and $\mu^+\mu^-$ channels. The values are shown in Tab. 7.

For $e^{\pm}\mu^{\mp}$ channel the simulation is corrected by a scale factor, drived from e^+e^- and $\mu^+\mu^-$ channels. $SF_{e\mu(1j1b)} = \sqrt{SF_{ee}.SF_{\mu\mu}(1j1b)} = 0.9 \pm 0.03$

Table 7: Drell-Yan background estimation for different levels of the event selection. The uncertainties are just statistical.

	e^+e^- channel	$\mu^+\mu^-$ channel	$e^\pm\mu^\mp$ channel
1j1b			
$N_{\ell\ell,in}(DYMC)$	72715.4 ± 713.59	163406 ± 1077.96	
$N_{\ell\ell,out}(DYMC)$	4874.96 ± 206.37	11744.9 ± 326.89	
$k_{\ell\ell}$	0.66 ± 0.002	1.5 ± 0.01	
$N_{\ell\ell,in}^{(obseved)}$	68120 ± 260.998	154526 ± 93.09	8085 ± 89.91
$N_{\ell\ell,out}^{(estimated)}$	4387.46 ± 185.36	10670.8 ± 306.571	
SF	0.90 ± 0.05	0.91 ± 0.03	0.9 ± 0.03
2j1b			
$N_{\ell\ell,in}(DYMC)$	26152 ± 444.68	57337.4 ± 695.92	
$N_{\ell\ell,out}(DYMC)$	2046.34 ± 140.36	4837.85 ± 227.08	
$k_{\ell\ell}$	0.67 ± 0.003	1.47 ± 0.01	
$N_{\ell\ell,in}^{(obseved)}$	31432 ± 177	68201 ± 261.15	10970 ± 104.73
$N_{\ell\ell,out}^{(estimated)}$	2171.85 ± 185.361	5074.15 ± 247.07	
SF	1.06 ± 0.1	1.04 ± 0.07	1.04 ± 0.09
2j2b			
$N_{\ell\ell,in}(DYMC)$	2391.41 ± 139.1	6246.76 ± 219.7	
$N_{\ell\ell,out}(DYMC)$	123.618 ± 140.36	418.09 ± 64.58	
$k_{\ell\ell}$	0.67 ± 0.008	1.47 ± 0.03	
$N_{\ell\ell,in}^{(obseved)}$	4512 ± 67.17	9868 ± 99.33	5796 ± 76.13
$N_{\ell\ell,out}^{(estimated)}$	132.86 ± 39.9	375.33 ± 59.95	
SF	1.07 ± 0.45	0.9 ± 0.1	0.98 ± 0.07
$\geq$ 2j, $\geq$1b			
$N_{\ell\ell,in}(DYMC)$	44785.6 ± 613.04	94189.1 ± 911.36	
$N_{\ell\ell,out}(DYMC)$	3473 ± 198.61	8169 ± 304.8	
$k_{\ell\ell}$	0.68 ± 0.002	1.46 ± 0.01	
$N_{\ell\ell,in}^{(obseved)}$	54540 ± 233.53	117331 ± 342.53	29837 ± 172.73
$N_{\ell\ell,out}^{(estimated)}$	3442.87 ± 203.31	8287.66 ± 321.08	
SF	0.99 ± 0.08	1.01 ± 0.05	0.99 ± 0.06

The value of SFs for the different levels of the selection (1j1b, 2j1b, 2j2b, $\geq$2j $\geq$1b) is summarized in Tab. 8. The corresponding uncertainties include the statistics uncertainties.

Table 8: Value of SF for the different levels. The uncertainties are just statistical.

Level	e^+e^- channel	$\mu^+\mu^-$ channel	$e^\pm\mu^\mp$ channel
1j1b	0.90 ± 0.05	0.91 ± 0.03	0.9 ± 0.03
2j1b	1.04 ± 0.07	1.06 ± 0.1	1.04 ± 0.09
2j2b	0.9 ± 0.1	1.07 ± 0.45	0.98 ± 0.07
$\geq$2j,$\geq$1b	1.01 ± 0.05	0.99 ± 0.08	0.99 ± 0.06

4.2 Non-W background

Non-W/Z backgrounds arise from processes with one prompt-lepton (decaying from a W or a Z boson) and one non-prompt lepton that passes the isolation and identification criteria. The latter will be also referred as a "fake lepton". Most of the events from such backgrounds are due to semi-leptonic $t\bar{t}$ and W+jets production, with some small contribution from single top and QCD events.

The fake lepton estimate is performed with the same-sign control region method. This method relies on a control region defined by the same criteria as the nominal signal region, but requiring same-sign dilepton pairs instead of opposite-sign ones. The control region is dominated by instrumental backgrounds (mainly fake leptons). The same-sign control region will also contain contributions from events with two prompt leptons and charge misidentification, and events with real same-sign pairs, such as those from $t\bar{t}V$ or WZ.

For estimating non W/Z background we use the same-sign event yields in data after substraction of the prompt-lepton same-sign contributions, multiplied by the ratio of opposite-sign over same-sign events coming from non-prompt lepton backgrounds. This ratio is taken purely from MC. The estimate is calculated using the following equation:

$$N_{data}^{OSfakes} = (N_{data}^{SS} - N_{real-pp}^{SS}) \cdot \frac{N_{MC}^{OSfakes}}{N_{MC}^{SSfakes}} \quad (1)$$

where N_{data}^{SS} is the number of SS events observed in data, $N_{real-pp}^{SS}$ is the expected number of real same-sign events, which also includes the expected number of same-sign events with charge misidentification, and $N_{MC}^{OSfakes}$ and $N_{MC}^{SSfakes}$ are the numbers of opposite-sign and same-sign events containing fake leptons observed in MC. This ratio of opposite-sign to same-sign events is called R, and is calculated from semi-leptonic $t\bar{t}$ and W+jets samples, as these processes are expected to produce the majority of the fake lepton background in this analysis. Table 9 shows the expected number of non-W/Z background events after the 1j1b, 2j1b and 2j2b tag requirement, as well as the number of events observed in the same-sign control region in data and the predicted fake lepton background. Table 9 also shows the non-W/Z background contribution to the event yields after applying all the selection cuts. The corresponding uncertainties include the statistics uncertainties.

Source	1j1b	2j1b	2j2b
Drell-Yan (SS)	31.7	39.1	0.0
Dibosons (SS)	21.8	12.4	0.0
$t\bar{t}$ V (SS)	7.3	24.1	6.5
$t\bar{t}$ dilepton (SS)	233.9	309.3	135.3
Single top quark (SS)	42.4	29.4	5.5
Total background (SS)	337.1 ± 18.4	414.3 ± 20.3	147.2 ± 12.1
Data (SS)	710.0 ± 26.6	910.0 ± 30.2	216.0 ± 14.7
SS data - bkg	372.9 ± 32.4	495.7 ± 36.4	68.8 ± 19.1
Non W/Z lep (SS)	285.5 ± 16.9	437.4 ± 20.9	22.7 ± 4.8
Non W/Z lep (OS)	197.9 ± 14.1	441.7 ± 21.0	78.0 ± 8.8
R (OS/SS)	0.69 ± 0.06	1.01 ± 0.07	3.44 ± 0.82
Non W/Z estimation	258.4 ± 31.7	500.6 ± 50.5	236.4 ± 86.5

Table 9: Non W/Z background estimation at the final level of selection.

5 Signal Extraction

After the event selection is performed, the data sample in the 1j1b region consists primarily of $t\bar{t}$ events with a significant number of tW signal events (see for example Fig. 9). In order to gain discrimination power, events with exactly 2 jets with one of them b tagged (2j1b region) show a reasonable signal to background ratio and are used separately to perform the signal extraction. Events with exactly 2 jets which are b tagged (2j2b), region highly enriched in $t\bar{t}$ events, are also used to constrain the main source of background.

As there is no single observable that clearly discriminates between the tW signal and the $t\bar{t}$ background, several observables are combined into a single discriminator using a BDT technique [50]. A collection of decision trees is created that weakly separates events into signal and background based on a number of binary decisions considering a single observable at a time. A boosting algorithm is then used to assign weights to each tree such that the ensemble of weak classifiers performs as a strong classifier [51]. In this analysis, the BDT implementation is provided by the tmva package [52], using the GradientBoost algorithm.

A multivariate analysis is used in order to provide discrimination between the tW signal and the main background process, $t\bar{t}$. Specifically, boosted decision trees (BDT) [50] are trained using the "Toolkit for Multivariate Data Analysis" (TMVA) [52]. Training of the BDT is done using dedicated dilepton samples for tW and $t\bar{t}$, which are listed in Tab. 3, in each one of the signal and control regions described above.

5.1 1 jet, 1 b-tag

The input variables used for the training of the BDT are the following:

- Number of loose jets ($20 < p_{\mathrm{T}} < 30$ GeV, $|\eta| < 2.4$)
- Number of b-tag loose jets ($20 < p_{\mathrm{T}} < 30$ GeV, $|\eta| < 2.4$ and CSVM b-tagged)
- p_T^{sys}: vector sum of p_{T} of leptons, jet, and $\not{E}_T$
- H_T: scalar sum of p_{T} of leptons, jet, and $\not{E}_T$
- Ratio of p_T^{sys} to H_T for the event
- p_{T} of the leading, tight, b-tagged jet
- p_{T} of leading loose jet, defined as 0 for events with no loose jets present

- M_{sys}: Invariant mass of the combination of the leptons, jet, and $\not{E}_T$
- Centrality (ratio between the transverse momentum and the total momentum) of the system of the jet and the two leptons,
- Ratio of scalar sum of p_T of the leptons to the H_T of full system
- Vector sum of p_T of jet and leptons

The BDTs are trained and tested using a dedicated set of Monte Carlo samples, different from the ones used for the signal extraction. As signal, the tW no-hadronic samples are used, while the dileptonic $t\bar{t}$ sample is used for background.

The training is performed with half of the available dataset, using the three decay modes: e^+e^-, $\mu^+\mu^-$ and $e^\pm\mu^\mp$. We trained two kinds of BDTs, using different boosting algorithms: adaptative boost and gradient boost, and have tuned the hyperparameters (learning rate, number of trees, maximum depth of the tree,...) to deliver the best performance in each case. This performance has been measured using the integral below the ROC curve as a figure-of-merit. The gradient boost is observed to deliver better results in general than the adaptative boost. The hyperparameters of the chosen BDT are shown in Tab. 10. The area under the ROC curve obtained for this BDT is 0.696.

Table 10: Hyperparameters of the BDT used in the 1j1b region.

Hyperparameter	Value
Number of trees	2000
Shrinkage (learning rate)	0.01
Maximum tree depth	4

Figs. 10 and 11 show a data-MC and signal-background comparison, respectively, of the input variables used for the training in this region. The relative importance of the input variables of the BDT in this region is shown in table 11.

Table 11: Relative importance of the input variables in the BDT used in the 1j1b region.

Variable	Relative importance
TTJetLooseCentralpt	$1.233 \cdot 10^{-1}$
TDilepMETJetPt	$1.099 \cdot 10^{-1}$
TTJet1$_p t$	$1.054 \cdot 10^{-1}$
THTLepOverHT	$1.029 \cdot 10^{-1}$
TnLooseCentral	$9.780 \cdot 10^{-2}$
TC$_j ll_v$2	$9.763 \cdot 10^{-2}$
TDilepJetPt	$9.305 \cdot 10^{-2}$
TTHTtot	$9.074 \cdot 10^{-2}$
TDilepMETJetPt$_T HTtot$	$8.054 \cdot 10^{-2}$
TMSys	$6.182 \cdot 10^{-2}$
TnBTotal	$3.692 \cdot 10^{-2}$

The shapes of the BDT discriminant for the training and testing samples of both the signal and background are shown in Fig. 12.

5.2 2 jets, 1 b-tag

The input variables used for the training of the BDT in the 2j1b region are the following:

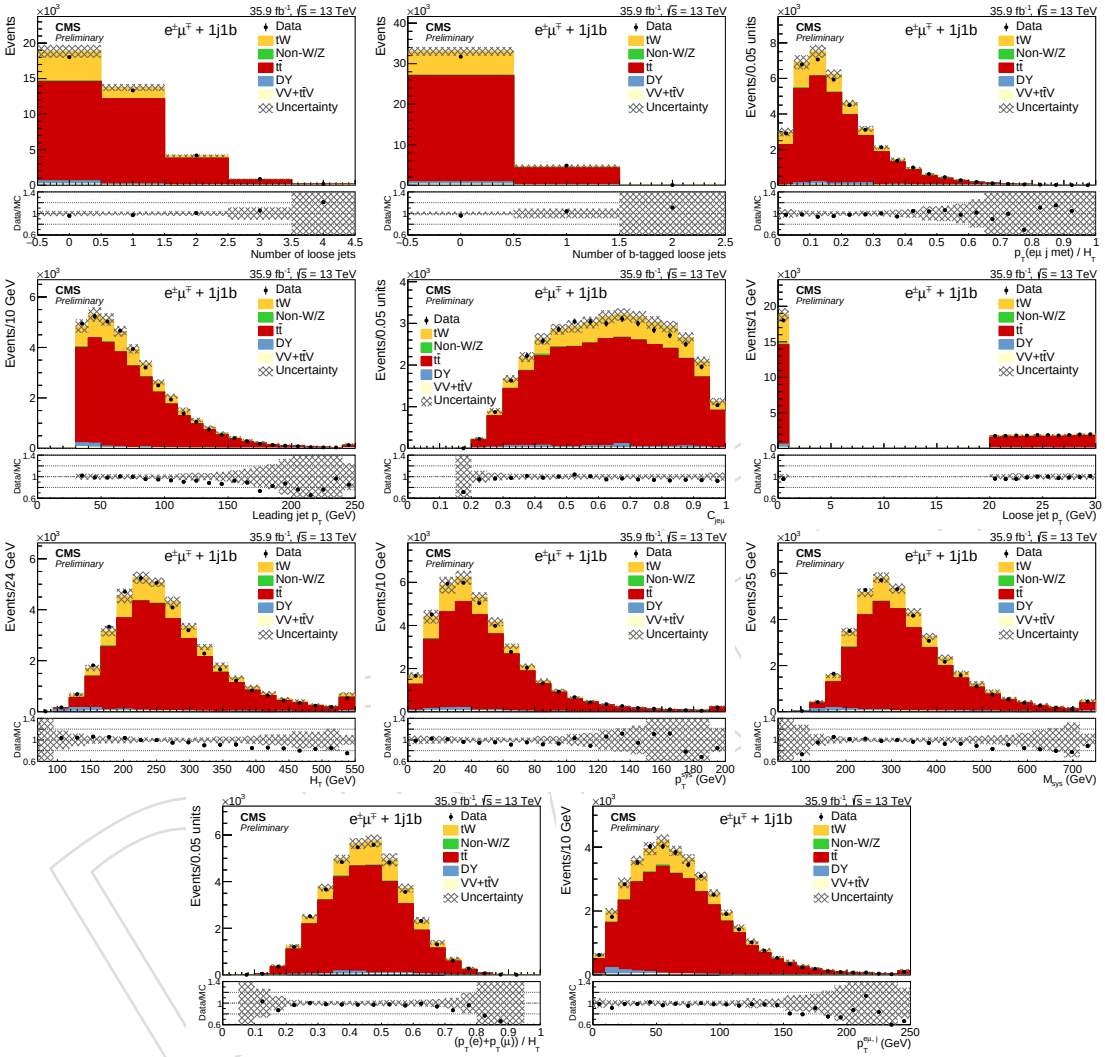

Figure 10: Data-MC comparison of the input variables used for the BDT in the 1j1b region. From top left to bottom right: number of loose jets, number of b-tag loose jets, ratio of p_T^{sys} to H_T, leading jet p_T, centrality of the jet and the leptons, loose jet p_T, H_T, p_T^{sys}, M_{sys}, ratio of scalar sum of p_T of the leptons to the H_T of full system and vector sum of p_T of the jet and the leptons.

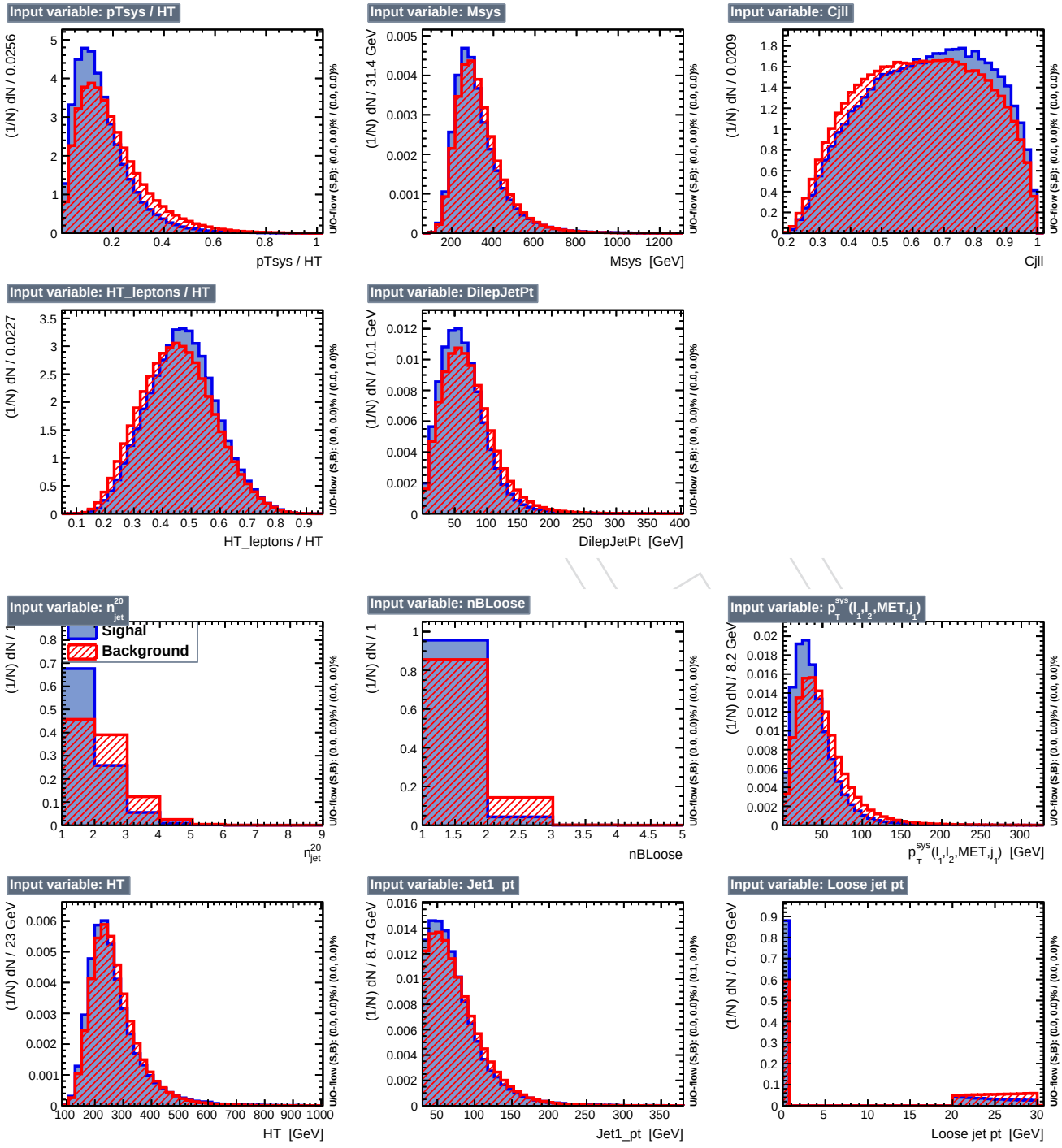

Figure 11: Signal-bkg comparison of the input variables used for the BDT in the 1j1b region. From top left to bottom right: number of loose jets, number of b-tag loose jets, p_T^{sys}, H_T, leading jet p_T, loose jet p_T, ratio of p_T^{sys} to H_T, M_{sys}, centrality of the jet and the leptons, ratio of scalar sum of p_T of the leptons to the H_T of full system, vector sum of p_T of the jet and the leptons.

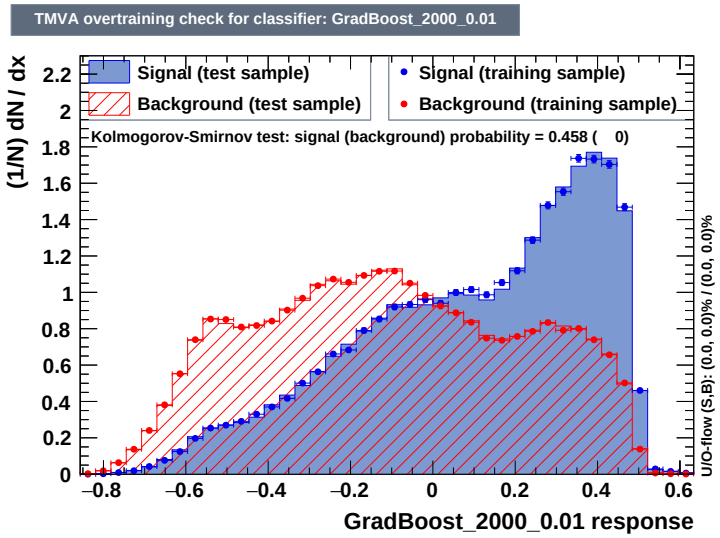

Figure 12: Signal-bkg comparison of the BDT output in the 1j1b signal region.

- p_{T} of the sub-leading jet
- $\Delta R(\ell_1, j_1)$: separation in $\phi - \eta$ space between the leading lepton and the leading jet.
- $\Delta R(\ell_1\ell_2, j_1j_2)$: separation in $\phi - \eta$ space between the dilepton and dijet system.
- $\Delta R(\ell_1\ell_2, j_1j_2E_T^{sys})$: separation in $\phi - \eta$ space between the dilepton and dijet and met system.

Figs. 13 and 14 show a data-MC and signal-background comparison, respectively, of the input variables used for the training in this region.

The shapes of the BDT discriminant for the training and testing samples of both the signal and background are shown in Fig. 15. The relative importance of the input variables used in the 2j1b BDT are showin in table 12.

Table 12: Relative importance of the input variables in the BDT used in the 2j1b region.

Variable	Relative importance
$\Delta R(\ell_1\ell_2; j_1j_2)$	$3.264{\cdot}10^{-1}$
$\Delta R(\ell_1\ell_2; METj_1j_2)$	$2.790{\cdot}10^{-1}$
$p_T^{j_2}$	$2.108{\cdot}10^{-1}$
$\Delta R(\ell_1, j_1)$	$1.838{\cdot}10^{-1}$

5.3 2 jets, 2 b-tags

As mentioned above, the main reason to use this category, highly enriched in $t\bar{t}$ events, is to constrain the main source of background. In order to that, the distribution of the p_{T} of the subleading jet is used. This is a variable sensitive to JES variations and, therefore, helpful to constrain this background.

5.4 Summary

Figure 16 shows the distributions of the BDT discriminants in the 1j1b and 2j1b regions, as well as the distribution of the p_T of the subleading jet in the 2j2b region to be used for the signal

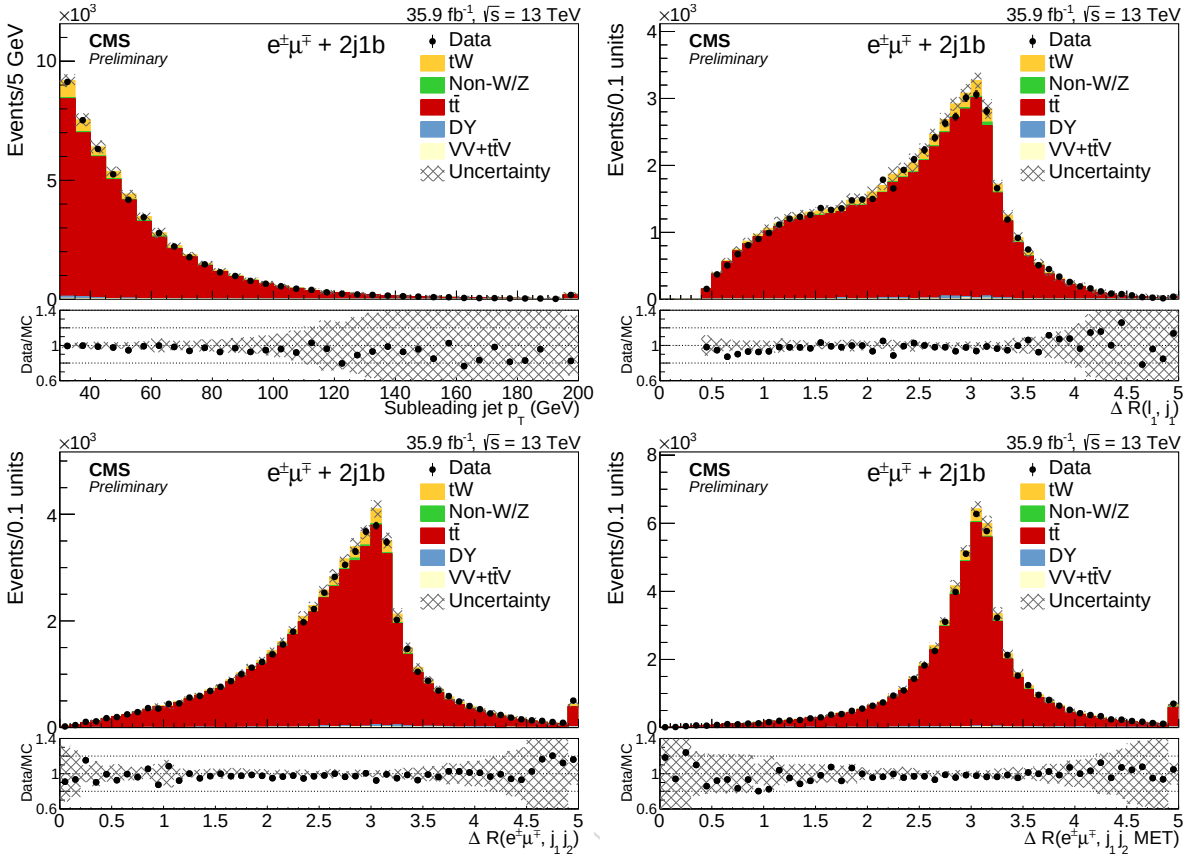

Figure 13: Data-MC comparison of the input variables used for the BDT in the 2j1b region. From top left to bottom right: p_{T} of the sub-leading jet, $\Delta R(\ell_1, j_1)$, $\Delta R(\ell_1\ell_2, j_1 j_2)$, $\Delta R(\ell_1\ell_2, j_1 j_2 E_T^{sys})$.

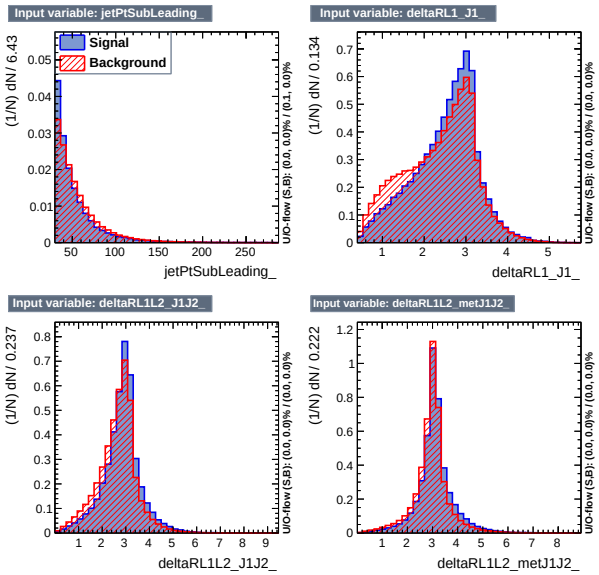

Figure 14: Signal-bkg comparison of the input variables used for the BDT in the 2j1b region. From top left to bottom right: p_{T} of the sub-leading jet, $\Delta R(\ell_1, j_1)$, $\Delta R(\ell_1\ell_2, j_1 j_2)$, $\Delta R(\ell_1\ell_2, j_1 j_2 E_T^{sys})$

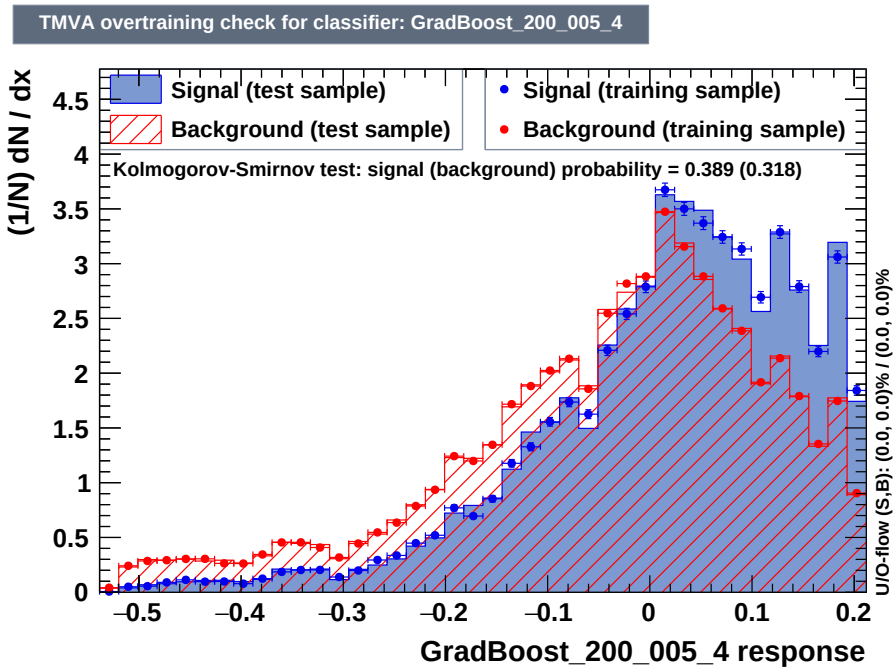

Figure 15: Signal-bkg comparison of the BDT output in the 2j1b signal region.

extraction. Other event categories are under study (see Appendix B) but are not used yet for the final result.

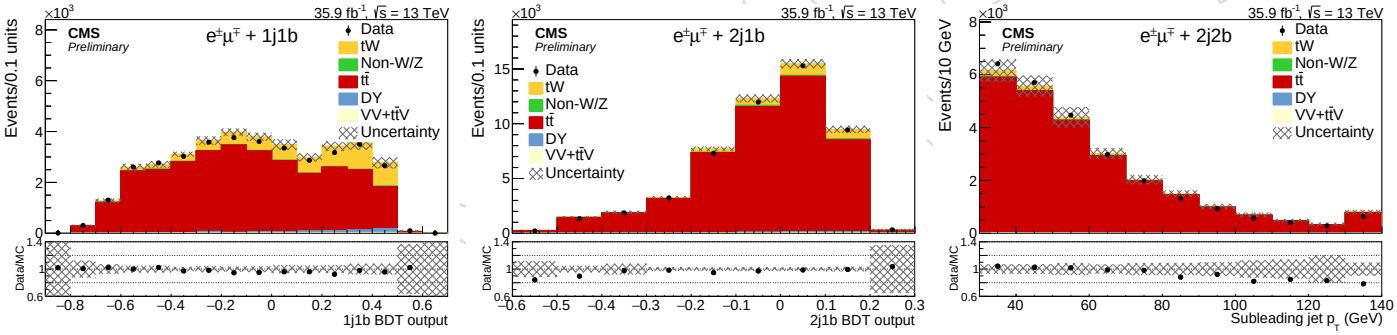

Figure 16: Data-MC comparison of the BDT output in the 1j1b (left) and 2j1b (right) regions and the p_{T} of the subleading jet in the 2j2b region .

6 Systematic uncertainties

The measurement of the tW production cross section is affected by systematic uncertainties that originate from detector effects and from theoretical assumptions. Each source of systematic uncertainty is assessed individually by suitable variations of the MC simulations or by variations of parameter values in the analysis within their estimated uncertainties.

6.1 Experimental uncertainties

- The uncertainties on the dilepton trigger (see Sect.3.4.2) and lepton identification efficiencies (see Sect. 3.4.3) in simulation are estimated by varying data-to-simulation

scale factors by their uncertainties. For muons, additional uncertainties of 1% for ID, 0.5% for Isolation and 0.5% for the single muon triggers are added in quadrature [47].

- The uncertainty due to the limited knowledge of the jet energy scale (JES) is usually determined by changes implemented in jet energy in bins of p_{T} and η, typically by a few percent [53].
- The uncertainty due to the limited accuracy of the jet energy resolution (JER) is determined by changing the JER correction from (1.109, 1.138, 1.114, 1.123, 1.084, 1.082, 1.140, 1.067, 1.177) for η bins (0.0 - 0.5, 0.5 - 0.8, 0.8 - 1.1, 1.1 - 1.3, 1.3 - 1.7, 1.7 - 1.9, 1.9 - 2.1, 2.1 - 2.3, 2.3 - 2.5) within their uncertainties (0.008, 0.013, 0.013, 0.024, 0.011, 0.035, 0.047, 0.053, 0.041), respectively [54, 55].
- The uncertainty due to the b-tagging efficiency is determined by varying the b-tagging scale factors derived at 13 TeV according to its uncertainty [49].
- The effect of pileup events is evaluated by weighting the simulation to the minimum bias cross section determined in data. The pileup model estimates the mean number of additional pp interactions to be about 20 events. These estimates are based on the total inelastic proton-proton cross section, which is determined to be 69.2 mb [45] at 13 TeV. The systematic uncertainty is estimated by varying the cross section within its uncertainty of $\pm$4.6%, changing the mean value by about one event.
- For ttV, VV, DY and nonW background contibutions, a conservative normalization uncertainty of $\pm$50% is assumed.
- The uncertainty on the integrated luminosity is currently estimated to be 2.5% [18].

6.2 Modeling Uncertainties

The modeling of the $t\bar{t}$ signal events by the MC simulation is an important ingredient in the measurement. The impact of theoretical assumptions in the modeling is determined by repeating the analysis and replacing the standard POWHEG +PYTHIA $t\bar{t}$ simulation by dedicated simulation samples with altered parameters.

The uncertainty on modeling of the hard-production process (ME scale) is assessed through changes in the renormalization and factorization scales in the POWHEG sample by factors of two and 0.5 relative to their common nominal value, which is set in POWHEG to $Q^2 = m_{\mathrm{t}}^2 + p_{\mathrm{T,t}}^2$, where $p_{\mathrm{T,t}}^2$ denotes the square transverse momentum of the top quark in the $t\bar{t}$ zero-momentum frame.

In order to take into account parton-shower (PS) uncertainties, different effects are studied:

- Underlying event: non-pertubative QCD effects are taken into account by tuning PYTHIA to measurements of the underlying event [21, 25]. The parameters of the tune are varied up and down within their uncertainties.
- ME/PS matching: the uncertainty in the combination of the matrix element calculation with the parton shower is estimated from the variation of the POWHEG parameter $h_{damp} = 1.58^{+0.66}_{-0.59} \cdot \mathrm{m}_t$. This parameter regulates the damping of real emissions in the NLO calculation when matching to the PS [21].
- Initial (final) state radiation scale: the PS scale used for the simulation of the initial (final) state radiation is varied up and down by a factor of two ($\sqrt{2}$).
- Color reconection: The effect of multiple-parton interactions and the parameterization of color reconnection have been studied in [25] and are varied accordingly. In addition, we use a simulation with activated color reconnection of resonant decays.

The uncertainties that arise from ambiguities in modeling color reconnection effects are estimated by comparing the default model in PYTHIA with two alternative models of color reconnection, a model with string formation beyond leading color [56] and a model in that the gluons can be moved to another string [57]. All models are tuned to measurements of the underlying event [21, 25]. In addition, the effects of color reconnection on the top decay products can be turned on in PYTHIA by enabling early resonance decays (turned off in the nominal sample).

The FSR uncertainty is modelled using three independent nuisance parameters, which affect separately to each region (1j1b, 2j1b and 2j2b).

The uncertainty from the choice of PDFs is determined by reweighting the sample of simulated $t\bar{t}$ events according to the 100 NNPDF3.0 error PDF sets [38].

Additionally, the difference between the diagram subtraction (DS) and diagram removal (DR) schemes is taken as a systematical uncertainty on the signal.

A detailed comparison of each systematic variation with respect to the nominal template is shown in Appendix A

7 Likelihood Fit

The signal is extracted by performing a maximum likelihood fit to data in several distributions. Fit templates for signal and background processes are taken from MC. The distributions of the BDT discriminants in the 1j1b and 2j1b regions, as well as the distribution of the p_T of the subleading jet in the 2j2b region are included in the fit. In order to do so, the signal strength parameter is defined as $\mu = \sigma/\sigma^{SM}$. Comparisons of the distribution of the BDT discriminants in the in the 1j1b and 2j1b regions as well as the distribution of the subleading jet in the 2j2b region for data and MC are shown in Fig. 17. In these distributions, the binning of the two BDT distributions is chosen in such a way that the $t\bar{t}$ background is uniform across the bins.

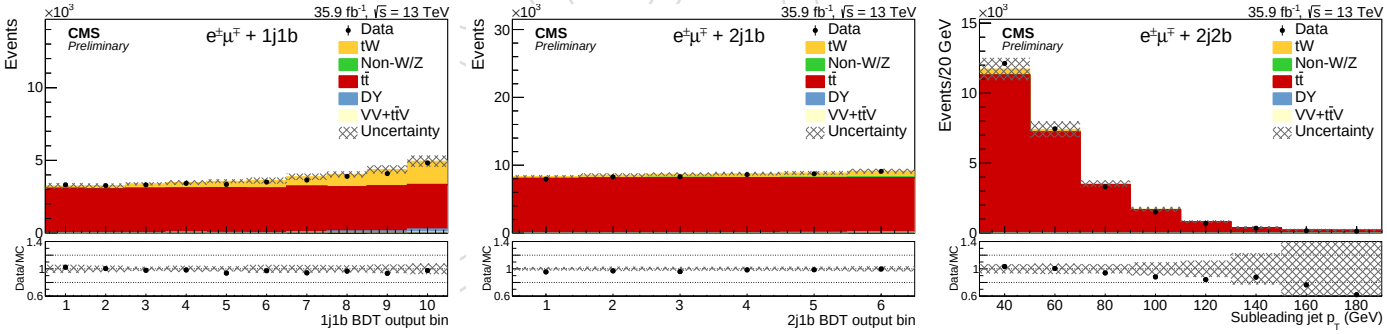

Figure 17: Data-MC comparison to the complete distribution to which the fit is performed.

The best fit to the data is obtained to be $0.88 \pm 0.02\,(\text{stat}) \pm 0.08\,(\text{syst}) \pm 0.03\,(\text{lum})$, corresponding to a measured cross-section of $63.1 \pm 1.8\,(\text{stat}) \pm 5.7\,(\text{syst}) \pm 2.1\,(\text{lum})$ pb and consistent with SM expectations. This result corresponds to an excess of 6.6 (8.3) observed (expected) standard deviations with respect to the no-signal hypothesis. Figure 18 shows the discriminant variable after the fit is performed.

Table 13 shows the expected significance of the signal when using different combination of event categories and dsitributions or just the plain in yields in some of these categories..

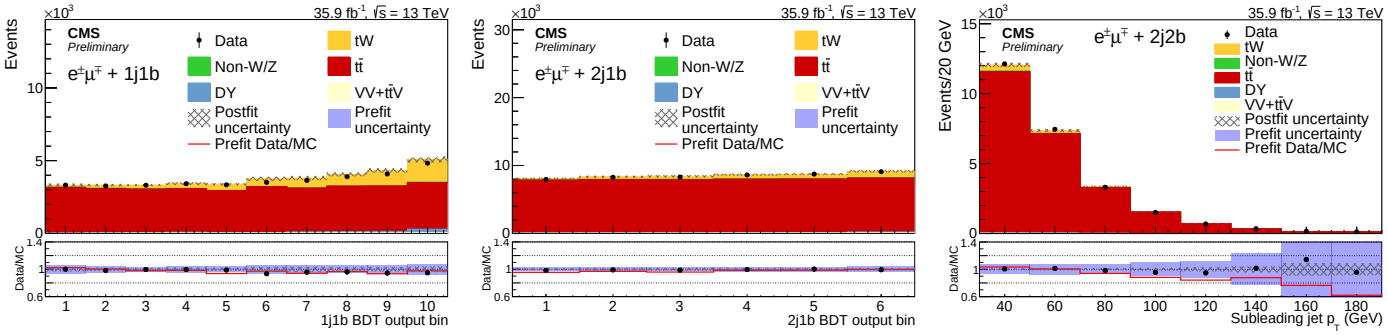

Figure 18: Data-MC comparison to the complete distribution after the fit is performed. Besides the Data-MC postfit ratio (black points), the Data-MC prefit ratio (red line) is shown in the ratio subplot, together with its uncertainty (blue).

Table 13: Expected sensitivity when using different regions.

Region	Expected significance (σ)
BDT 1j1b	3.5
BDT 1j1b + BDT 2j1b	4.8
Yields 1j1b + yields 2j1b + yields 2j2b	2.9
BDT 1j1b + yields 2j1b + yields 2j2b	4.3
BDT 1j1b + BDT 2j1b + yields 2j2b	5.8
BDT 1j1b + BDT 2j1b + shape 2j2b	8.3

Table 14 shows the contribution from the statistical component and each systematical uncertainty to the total uncertainty of the fit. The former contribution is obtained by reperforming the fit by fixing every nuisance parameter to its post-fit value, and evaluating the resulting uncertainty associated to the new fit. The contribution of a given systematical uncertainty is obtained by reperforming the fit by fixing every nuisance parameter to its post-fit value, and subtracting in quadrature the statistical component to the result.

8 Summary

An excess of events compared to a background only hypothesis is observed based on the fit to the data as described in the previous section with a significance of 6.6 σ, compared to an SM expectation of 8.3 standard deviations.

The best fit value for the signal corresponds to a signal strength of $0.88 \pm 0.02\,(\text{stat}) \pm 0.08\,(\text{syst}) \pm 0.03\,(\text{lum})$, yielding to a total cross-section measurement of $63.1 \pm 1.8\,(\text{stat}) \pm 5.7\,(\text{syst}) \pm 2.1\,(\text{lum})$ pb.

9 To do list

- Study the potential improvement of adding the 0j and 1j0b region
- Estimate the fiducial cross section

Table 14: Estimation of the effect of each systematical uncertainty to the fit. The quadratic sum of the separated contributions is 8.9 %, slightly differing to the total systematical uncertainty quoted, due to postfit correlations in the nuisances.

Source	Uncertainty (%)
Trigger efficiencies	2.7
Muon efficiencies	3.1
Electron efficiencies	3.2
Jet energy scale	3.2
Jet energy resolution	1.8
b tagging	1.4
Mistagging	0.2
Pileup	3.3
μ_R and μ_F scale	2.7
Underlying event	0.4
ME/PS matching	1.8
Initial state radiation	0.8
Final state radiation	0.8
Color reconnection	2.0
PDF	1.5
DR-DS	1.3
VV	0.4
Drell–Yan	1.1
Non-W/Z leptons	1.6
*tbar*V	0.1
MC statistics	1.6
Total systematic (no integrated luminosity)	9.1
Integrated luminosity	3.3
Statistical	2.8
Total	10.1

Acknowledgments

The authors would like to acknowledge the CMS electron and muon POGs for providing the lepton scale factors and corresponding uncertainties, and Till Arndt *et al*. for providing the trigger scale factor ans associated uncertainties. These are precious inputs used in the anlysis described here.

References

[1] CDF Collaboration, "First Observation of Electroweak Single Top Quark Production", *Phys. Rev. Lett.* **103** (2009) 092002, doi:10.1103/PhysRevLett.103.092002, arXiv:0903.0885.

[2] D0 Collaboration, "Observation of Single Top Quark Production", *Phys. Rev. Lett.* **103** (2009) 092001, doi:10.1103/PhysRevLett.103.092001, arXiv:0903.0850.

[3] S. Frixione et al., "Single-top hadroproduction in association with a W boson", *JHEP* **07** (2008) 029, doi:10.1088/1126-6708/2008/07/029, arXiv:0805.3067.

[4] A. S. Belyaev, E. E. Boos, and L. V. Dudko, "Single top quark at future hadron colliders: Complete signal and background study", *Phys. Rev.* **D59** (1999) 075001, doi:10.1103/PhysRevD.59.075001, arXiv:hep-ph/9806332.

[5] C. D. White, S. Frixione, E. Laenen, and F. Maltoni, "Isolating Wt production at the LHC", *JHEP* **11** (2009) 074, doi:10.1088/1126-6708/2009/11/074, arXiv:0908.0631.

[6] T. M. P. Tait and C. P. Yuan, "Single top quark production as a window to physics beyond the standard model", *Phys. Rev.* **D63** (2000) 014018, doi:10.1103/PhysRevD.63.014018, arXiv:hep-ph/0007298.

[7] Q.-H. Cao, J. Wudka, and C. P. Yuan, "Search for new physics via single top production at the LHC", *Phys. Lett.* **B658** (2007) 50–56, doi:10.1016/j.physletb.2007.10.057, arXiv:0704.2809.

[8] V. Barger, M. McCaskey, and G. Shaughnessy, "Single top and Higgs associated production at the LHC", *Phys. Rev. D* **81** (Feb, 2010) 034020, doi:10.1103/PhysRevD.81.034020.

[9] CMS Collaboration, "Evidence for associated production of a single top quark and W boson in pp collisions at $\sqrt{s}$ = 7 TeV", *Phys. Rev. Lett.* **110** (2013) 022003, doi:10.1103/PhysRevLett.110.022003, arXiv:1209.3489.

[10] ATLAS Collaboration, "Evidence for the associated production of a W boson and a top quark in ATLAS at $\sqrt{s} = 7$ TeV", *Phys. Lett.* **B716** (2012) 142–159, doi:10.1016/j.physletb.2012.08.011, arXiv:1205.5764.

[11] CMS Collaboration, "Observation of the associated production of a single top quark and a W boson in pp collisions at $\sqrt{s}$ =8 TeV", *Phys. Rev. Lett.* **112** (2014), no. 23, 231802, doi:10.1103/PhysRevLett.112.231802, arXiv:1401.2942.

[12] ATLAS Collaboration, "Measurement of the production cross-section of a single top quark in association with a W boson at 8 TeV with the ATLAS experiment", *JHEP* **01** (2016) 064, doi:10.1007/JHEP01(2016)064, arXiv:1510.03752.

[13] ATLAS Collaboration, "Measurement of the cross-section for producing a W boson in association with a single top quark in pp collisions at $\sqrt{s} = 13$TeV with ATLAS", arXiv:1612.07231.

[14] N. Kidonakis, "Theoretical results for electroweak-boson and single-top production", *PoS* **DIS2015** (2015) 170, arXiv:1506.04072.

[15] A. S. Belyaev, E. E. Boos, and L. V. Dudko, "Single top quark at future hadron colliders: Complete signal and background study", *Phys. Rev. D* **59** (Feb, 1999) 075001, doi:10.1103/PhysRevD.59.075001.

[16] T. M. P. Tait, "tW^-", *Phys. Rev. D* **61** (Dec, 1999) 034001, doi:10.1103/PhysRevD.61.034001.

[17] JSON file: /afs/cern.ch/cms/CAF/CMSCOMM/COMM_DQM/certification/Collisions16/13TeV/ReReco/Final/Cert_271036-284044_13TeV_23Sep2016ReReco_Collisions16_JSON.txt.

[18] CMS Collaboration, "CMS Luminosity Measurements at 13 TeV - Winter 2017 update", *Physics Analysis Summary* **CMS-PAS-LUMI-17-001** (2017).

[19] E. Re, "Single-top Wt-channel production matched with parton showers using the POWHEG method", *Eur. Phys. J. C* **71** (2011) 1547, doi:10.1140/epjc/s10052-011-1547-z, arXiv:1009.2450.

[20] CMS Collaboration, "Underlying Event Tunes and Double Parton Scattering", Technical Report CMS-PAS-GEN-14-001, CERN, Geneva, 2014.

[21] P. Skands, S. Carrazza, and J. Rojo, "Tuning PYTHIA 8.1: the Monash 2013 Tune", *Eur. Phys. J.* **C74** (2014), no. 8, 3024, doi:10.1140/epjc/s10052-014-3024-y, arXiv:1404.5630.

[22] S. Alioli et al., "A general framework for implementing NLO calculations in shower Monte Carlo programs: the POWHEG BOX", *JHEP* **06** (2010) 043, doi:10.1007/JHEP06(2010)043, arXiv:1002.2581.

[23] T. Sjöstrand, S. Mrenna, and P. Skands, "PYTHIA 6.4 physics and manual", *JHEP* **05** (2006) 026, doi:10.1088/1126-6708/2006/05/026, arXiv:hep-ph/0603175.

[24] T. Sjostrand et al., "An Introduction to PYTHIA 8.2", *Comput. Phys. Commun.* **191** (2015) 159–177, doi:10.1016/j.cpc.2015.01.024, arXiv:1410.3012.

[25] CMS Collaboration, "Investigations of the impact of the parton shower tuning in Pythia 8 in the modelling of $\mathrm{t\bar{t}}$ at $\sqrt{s} = 8$ and 13 TeV", Technical Report CMS-PAS-TOP-16-021, CERN, Geneva, 2016.

[26] M. Bahr et al., "Herwig++ Physics and Manual", *Eur. Phys. J.* **C58** (2008) 639–707, doi:10.1140/epjc/s10052-008-0798-9, arXiv:0803.0883.

[27] J. Alwall et al., "The automated computation of tree-level and next-to-leading order differential cross sections, and their matching to parton shower simulations", *JHEP* **07** (2014) 079, doi:10.1007/JHEP07(2014)079, arXiv:1405.0301.

[28] P. Artoisenet et al., "Automatic spin-entangled decays of heavy resonances in Monte Carlo simulations", *JHEP* **03** (2013) 015, doi:10.1007/JHEP03(2013)015, arXiv:1212.3460.

[29] NNPDF Collaboration, "Parton distributions with LHC data", *Nucl. Phys. B* **867** (2013) 244, doi:10.1016/j.nuclphysb.2012.10.003, arXiv:1207.1303.

[30] R. Frederix and S. Frixione, "Merging meets matching in MC@NLO", *JHEP* **12** (2012) 061, doi:10.1007/JHEP12(2012)061, arXiv:1209.6215.

[31] N. Kidonakis, "Two-loop soft anomalous dimensions for single top quark associated production with $\mathrm{W^-}$ or $\mathrm{H^-}$", *Phys. Rev. D* **82** (2010) 054018, doi:10.1103/PhysRevD.82.054018, arXiv:hep-ph/1005.4451.

[32] J. M. Campbell, R. K. Ellis, and C. Williams, "Vector boson pair production at the LHC", *JHEP* **07** (2011) 018, doi:10.1007/JHEP07(2011)018, arXiv:1105.0020.

[33] M. Czakon and A. Mitov, "Top++: A Program for the Calculation of the Top-Pair Cross-Section at Hadron Colliders", *Comput.Phys.Commun.* **185** (2014) 2930, doi:10.1016/j.cpc.2014.06.021, arXiv:1112.5675.

[34] S. Alekhin et al., "The PDF4LHC Working Group Interim Report", arXiv:1101.0536.

[35] M. Botje et al., "The PDF4LHC Working Group Interim Recommendations", arXiv:1101.0538.

[36] A. D. Martin, W. J. Stirling, R. S. Thorne, and G. Watt, "Parton distributions for the LHC", *Eur. Phys. J. C* **63** (2009) 189, doi:10.1140/epjc/s10052-009-1072-5, arXiv:0901.0002.

[37] H.-L. Lai et al., "New parton distributions for collider physics", *Phys. Rev. D* **82** (2010) 074024, doi:10.1103/PhysRevD.82.074024, arXiv:1007.2241.

[38] J. Gao et al., "CT10 next-to-next-to-leading order global analysis of QCD", *Phys. Rev. D* **89** (2014) 033009, doi:10.1103/PhysRevD.89.033009, arXiv:1302.6246.

[39] CMS Collaboration, "Particle-flow reconstruction and global event description with the CMS detector", arXiv:1706.04965.

[40] https://twiki.cern.ch/twiki/bin/viewauth/CMS/CutBasedElectronIdentificationRun2.

[41] https://twiki.cern.ch/twiki/bin/view/CMS/SWGuideMuonIdRun2#Tight_Muon.

[42] https://twiki.cern.ch/twiki/bin/viewauth/CMS/JetID#Recommendations_for_13_TeV_2016.

[43] https://twiki.cern.ch/twiki/bin/viewauth/CMS/MissingETOptionalFiltersRun2.

[44] CMS collaboration Collaboration, "Site: https://twiki.cern.ch/twiki/bin/view/CMS/TWikiTopRefEventSel",.

[45] https://twiki.cern.ch/twiki/bin/viewauth/CMS/PileupJSONFileforData.

[46] T. Arndt et al., "Measurement of the 2016 Trigger Efficiencies for a dilepton Selection for a $t\bar{t}$ analysis", *CMS AN-2016/392* (2016).

[47] https://twiki.cern.ch/twiki/bin/viewauth/CMS/MuonReferenceEffsRun2.

[48] https://twiki.cern.ch/twiki/bin/viewauth/CMS/EgammaIDRecipesRun2#Cut_based_electron_identificatio.

[49] https://twiki.cern.ch/twiki/bin/viewauth/CMS/BtagRecommendation#Recommendation_for_13_TeV_Data.

[50] J. H. Friedman, "Stochastic gradient boosting", *Computational Statistics & Data Analysis* **38** (2002), no. 4, 367 – 378, doi:https://doi.org/10.1016/S0167-9473(01)00065-2. Nonlinear Methods and Data Mining.

[51] R. E. Schapire, "The strength of weak learnability", *Machine Learning* **5** (1990), no. 2, 197–227, doi:10.1007/BF00116037.

[52] H. Voss, A. Höcker, J. Stelzer, and F. Tegenfeldt, "TMVA, the Toolkit for Multivariate Data Analysis with ROOT", in *XI International Workshop on Advanced Computing and Analysis Techniques in Physics Research*, p. 040. SISSA, 2007. arXiv:physics/0703039. PoS(ACAT2007)040.

[53] CMS Collaboration, "Jet energy scale and resolution in the CMS experiment in pp collisions at 8 TeV", *JINST* **12** (2017), no. 02, P02014, doi:10.1088/1748-0221/12/02/P02014, arXiv:1607.03663.

[54] CMS Collaboration Collaboration, "Jet algorithms performance in 13 TeV data", Technical Report CMS-PAS-JME-16-003, CERN, Geneva, 2017.

[55] https://twiki.cern.ch/twiki/bin/viewauth/CMS/JetResolution#JER_Scaling_factors_and_Uncertai.

[56] J. R. Christiansen and P. Z. Skands, "String Formation Beyond Leading Colour", *JHEP* **08** (2015) 003, doi:10.1007/JHEP08(2015)003, arXiv:1505.01681.

[57] S. Argyropoulos and T. Sjstrand, "Effects of color reconnection on $t\bar{t}$ final states at the LHC", *JHEP* **11** (2014) 043, doi:10.1007/JHEP11(2014)043, arXiv:1407.6653.

A Systematic variations

This section shows the variations of the discriminant variable due to the different sistematic uncertainties on tW (Figs. 19 and 20) and $t\bar{t}$ (Figs. 21 and 22) events.

The overall variations of each systematic uncertainty with respect to the nominal $t\bar{t}$ sample is shown in Tab. 15.

Table 15: Variations in $t\bar{t}$ events of each systematic source in the 3 regions.

	2j2b up	2j2b down	2j1b up	2j1b down	1j1b up	1j1b down
FSR	-10.06	5.43	-0.20	2.28	0.57	-0.00
ISR	-2.13	0.09	-1.33	1.76	-0.40	1.62
Color	1.03	-2.74	1.13	-0.71	0.59	-1.75
Scale	0.94	-1.99	0.56	-1.20	0.71	-1.71
PDF	0.77	-0.77	0.73	-0.73	1.24	-1.24
UE	-0.94	-0.66	-0.21	0.03	0.80	-0.12
JES	-0.34	0.17	-0.10	0.04	-3.48	3.54
JER	-0.90	0.90	-0.26	0.26	-0.32	0.32
BTAG	3.37	-3.37	0.04	-0.04	1.52	-1.52
hdamp	-1.56	2.81	-0.23	1.64	-1.50	3.83
MisTag	0.08	-0.08	-0.01	0.01	0.02	-0.02
PU	-0.73	0.72	-0.39	0.36	-0.60	0.58

B 0 jet and 1 jet 0 b-tags

Section under study and not finalized, work is in progress. Two additional regions, in which events are required to contain no jets (0j) or one non b-tagged jet (1j0b) and no b-tagged jets, which are rich in Drell-Yan events, are used to further constrain that background, as it is expected to contain only a small fraction of signal events.

The input variables used for the training of the BDT in the 0j and 1j0b regions are the following:

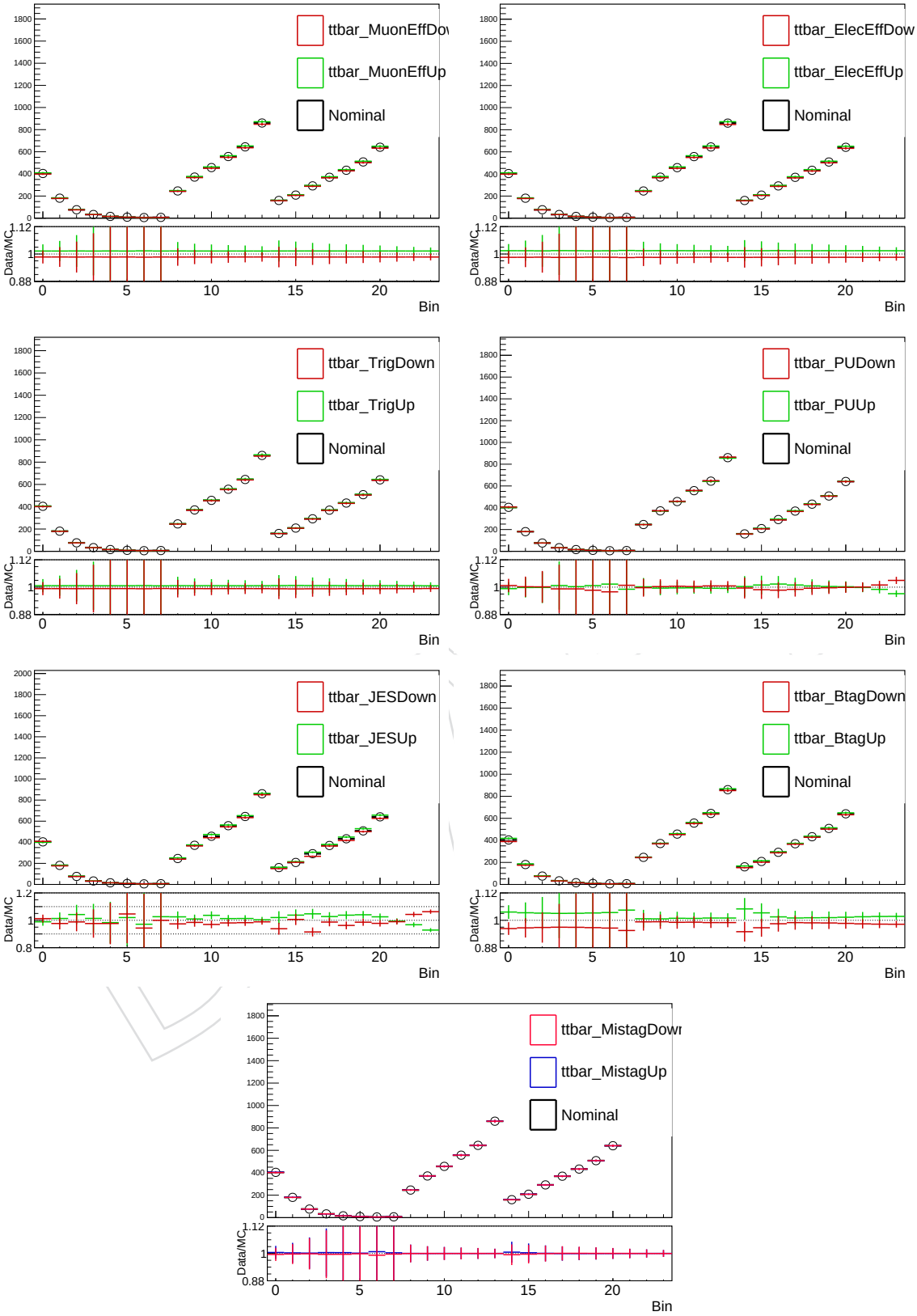

Figure 19: Experimental systematic variantios in tW events.

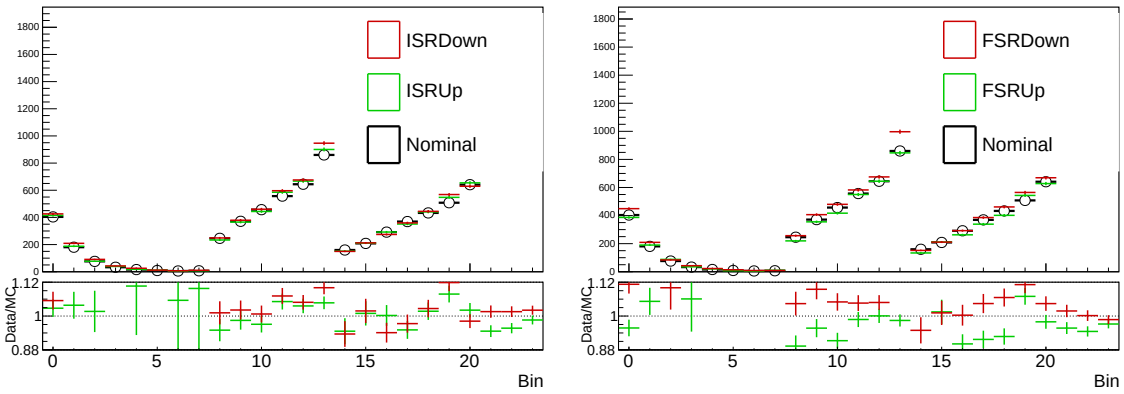

Figure 20: Modeling systematic variantios in tW events.

- $\not{E}_T$
- p_T of vector sum of momentums of two leptons, $\not{E}_T$and jet
- $p_T(\ell_1 + \ell_2) - p_T(\not{E}_T + \text{jet})$
- $p_T(\ell_1 + \ell_2) - p_T(\not{E}_T)$
- $p_T(\ell_1 + \text{jet} + \not{E}_T)$
- $M_{\ell_1\ell_2}$
- centrality of dilepton system ($c = E_T/p_T$)
- $p_T(\ell_1) - \not{E}_T)$
- H_T (scalar sum of p_T) of system
- $p_T(\text{jet})$
- $p_T(system)/H_T(system)$
- $M(system)$
- $p_T(\ell_1 + \ell_2 + \text{jet})$
- $H_T(\ell_1 + \ell_2)/H_T(system)$
- $p_T(\ell_1 + \ell_2)$
- $\Delta R(\ell_1 + \ell_2, \not{E}_T + \text{jet})$
- $\Delta R(\ell_1 + \ell_2, \text{jet})$
- $p_T(\ell_1) - p_T(\text{jet})$
- $M(\ell_1 + \text{jet})$
- $p_T(\ell_1)$
- $\Delta R(\ell_1, \text{jet})$
- b-tag of the leading jet

C Fit correlation matrices and pulls

Figure 23 show the post-fit pulls of the nuisance paramenters.

Figure 24 shows the post-fit correlation matrix of the parameters involved in the fit. Figure 24 also shows a reduced version of the matrix in which only the parameters not associated to Monte Carlo statistics are shown.

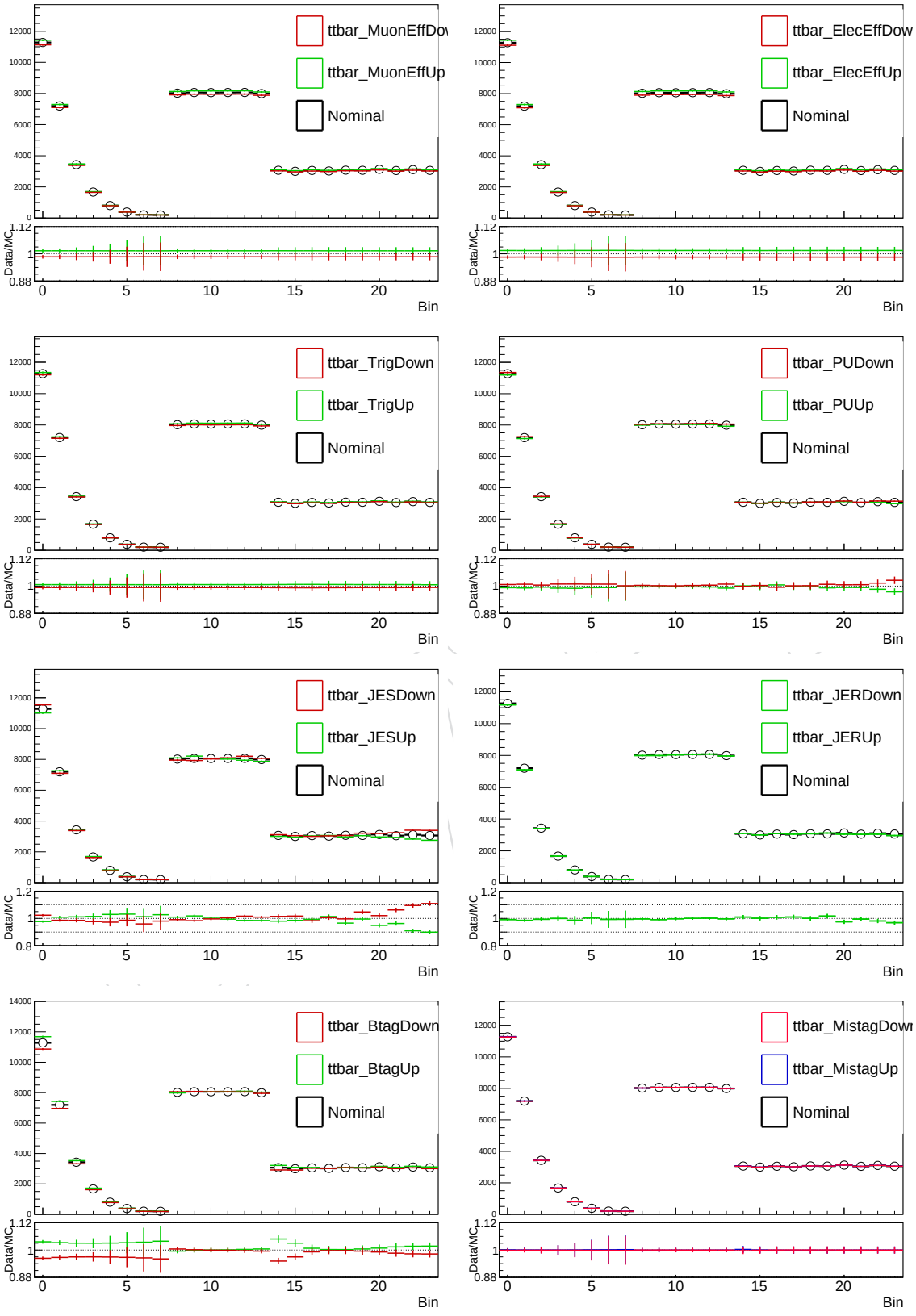

Figure 21: Experimental systematic variantios in $t\bar{t}$ events.

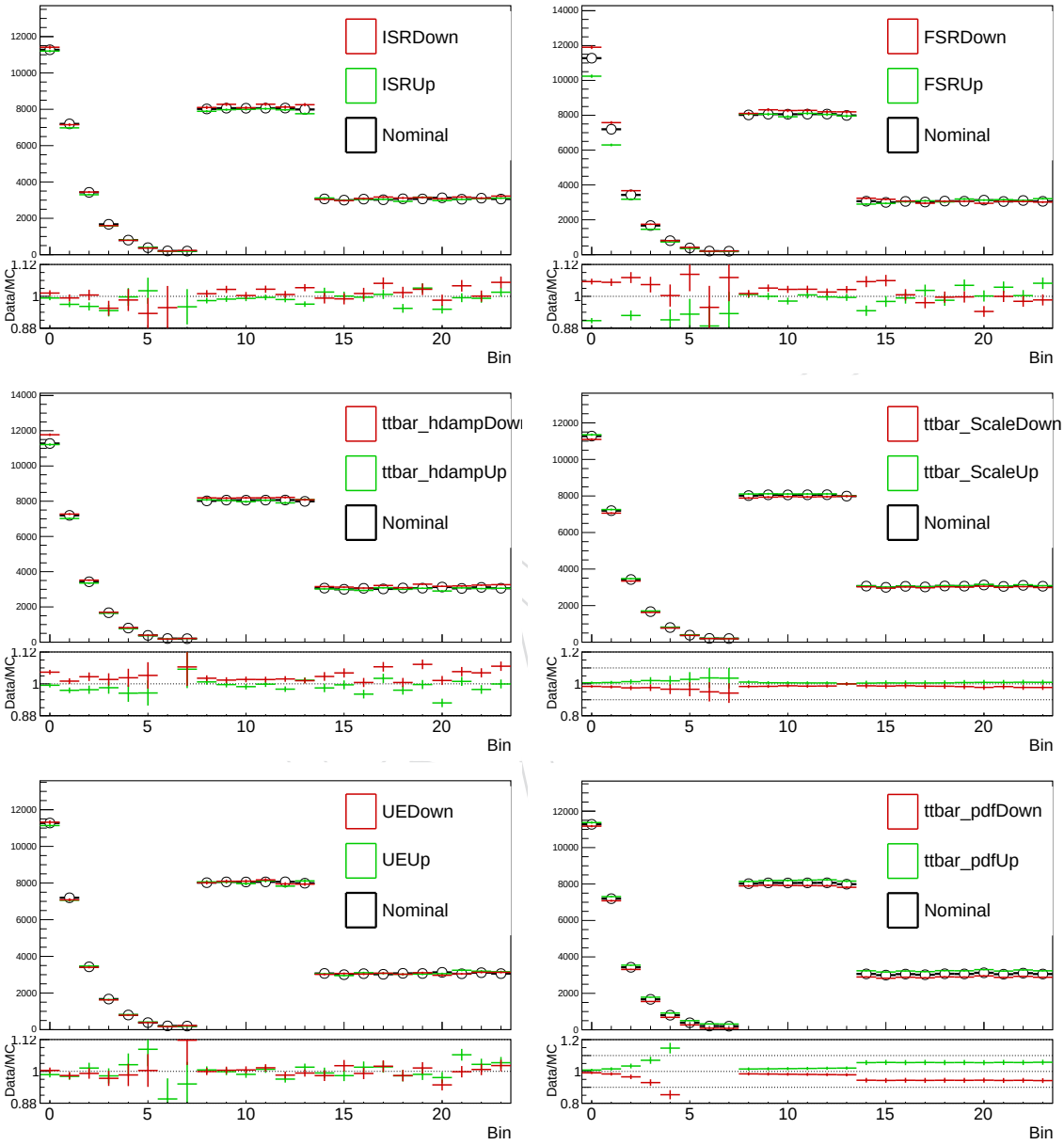

Figure 22: Modeling systematic variantios in $t\bar{t}$ events.

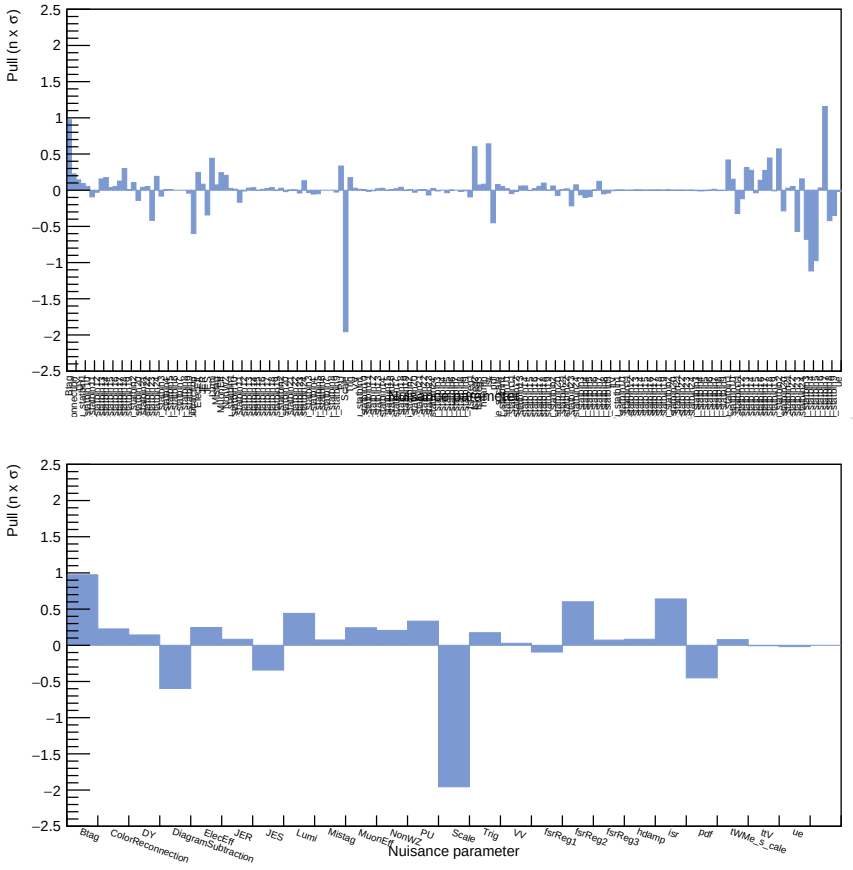

Figure 23: Post-fit pulls of all the nuisance parameters involved in the likelihood fit (top). Post-fit pulls of all nuisance parameters but the ones associated to Monte Carlo statistics (bottom).

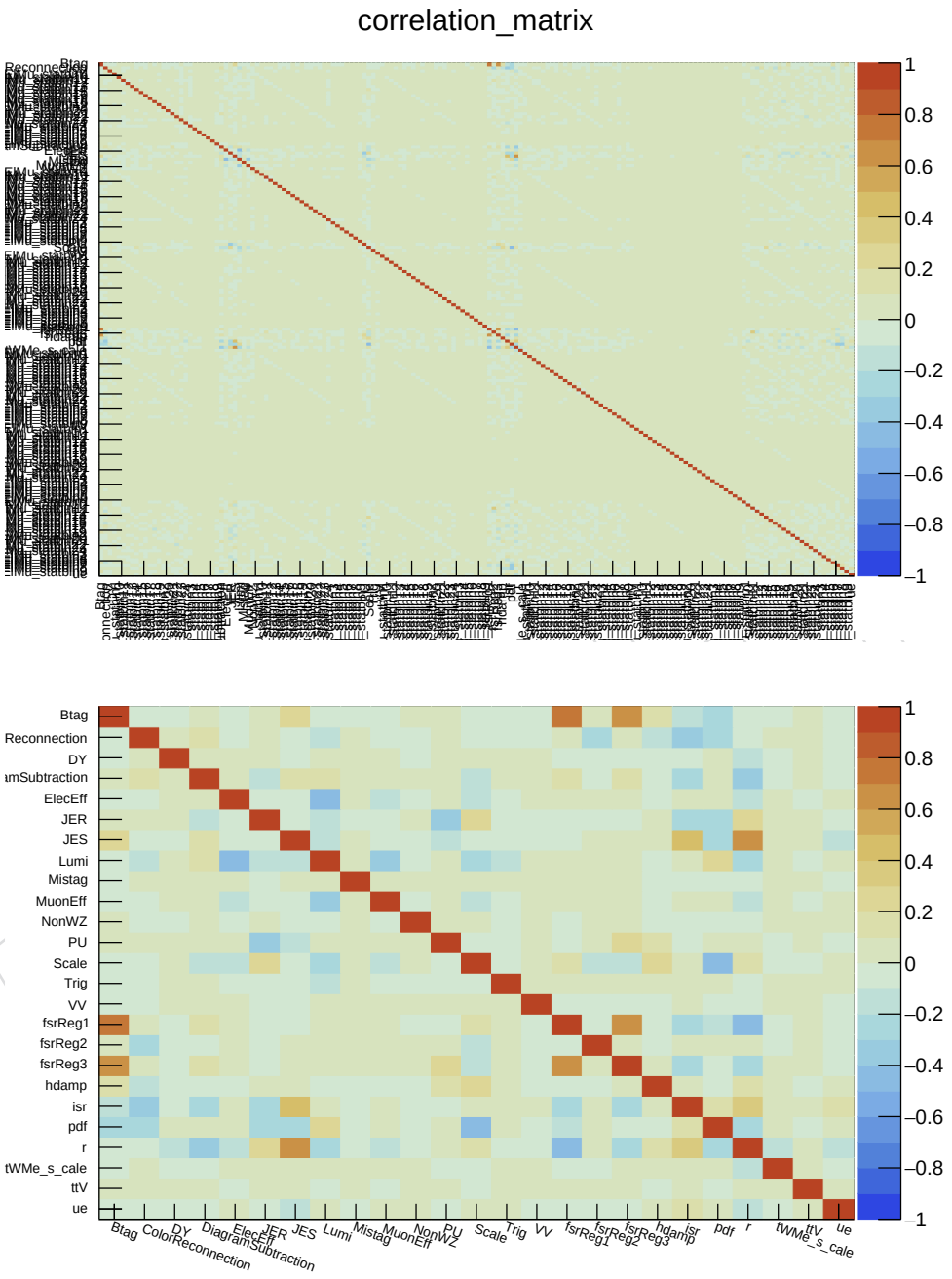

Figure 24: Post-fit correlation matrix of the parameters involved in the fit (top). The reduced version of this matrix, showing only paremeters not related to MC statistics is shown in the bottom.

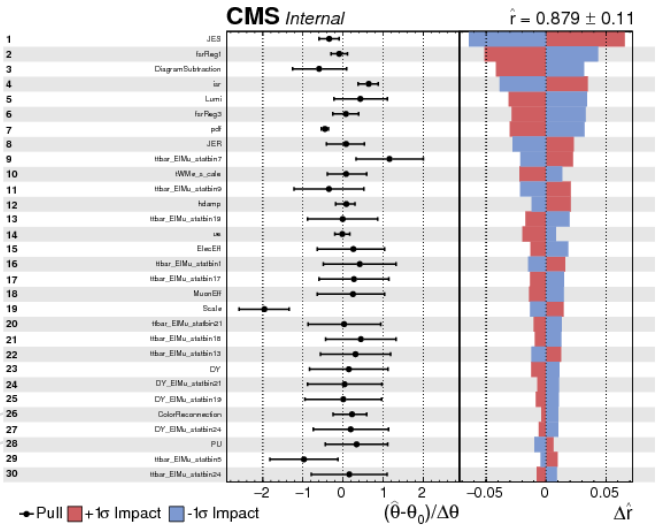

Figure 25: Impact plot of the fit.